UNIVERSITY OF SÃO PAULO
SÃO CARLOS INSTITUTE OF PHYSICS

ANDRES DAVID PEÑA UNIGARRO

Implementation and simulation of drift-diffusion models for organic mixed conductor devices

São Carlos
2022

ANDRES DAVID PEÑA UNIGARRO

Implementation and simulation of drift-diffusion models for organic mixed conductor devices

Dissertation presented to the Graduate Program in Physics at São Carlos Institute of Physics, University of São Paulo to obtain the degree of Master of Science.
Concentration area: Applied Physics.
Advisor: Dr. Florian Steffen Günther.
Co-advisor: Prof. Dr. Gregório Couto Faria.

Original Version

São Carlos
2022

Peña Unigarro, Andres David
Implementation and simulation of drift-diffusion models for organic mixed conductor devices / Andres David Peña Unigarro; advisor Florian Steffen Günther; co-advisor Gregório Couto Faria -- São Carlos 2022.
84 p.

Dissertation (Master's degree - Graduate Program in Theoretical and Experimental Physics) -- Instituto de Física de São Carlos, Universidade de São Paulo - Brasil , 2022.

1. Finite differences. 2. OECT. 3. Organic electronics. 4. Drift-diffusion. I. Günther, Florian Steffen , advisor. II. Faria, Gregório Couto, co-advisor. III. Title.

FOLHA DE APROVAÇÃO

Andres David Peña Unigarro

Dissertação apresentada ao Instituto de Física de São Carlos da Universidade de São Paulo para obtenção do título de Mestre em Ciências. Área de Concentração: Física Teórica e Experimental.

Aprovado(a) em: 09/05/2022

Comissão Julgadora

Dr(a). Florian Steffen Günther

Instituição: (IFSC/USP)

Dr(a). Lucas Fugikawa Santos

Instituição: (UNESP/Rio Claro)

Dr(a). Douglas José Coutinho

Instituição: (UTFPR/Curitiba)

Acknowledgements

The realization of this work was possible thanks to the contributions of many people, to whom I would like to give my most sincere acknowledgement. Each one was part of this important process, and contributed directly or indirectly to this step of my academic life. I would first like to thank my supervisor Florian Günther, who guided throughout this work, and whose support and dedication made me persist and always seek the best of myself. Much more than an advisor, he was a friend, and also a counselor, who made the realization and completion of this project possible.

I want to thanks to Gregorio Faria for the advice and mainly for the trust given to me, for his constant support during this important step in my life and for giving me the opportunity to be part of the polymer research group.

I am especially grateful to the São Carlos Institute of Physics for providing the financial support and making possible the execution of my master's project.

Furthermore, I am thankful to the friends I made during my master's period, with which shared good times in these two years. Although many people were present during this important time in my life, a special thanks goes to German, James, Rafael, Laureano, Bianca. Thank you for the support and the good times shared. All the talks and experiences during this time made my time in Brazil very pleasant and enriching. I will remember every moment shared with much affection and gratitude.

Finally, I would like to thank my family members. Particularly, to my parents and brother, who helped me and gave me constant support in all my decisions. Also, for the trust that my family placed in me during my academic career, which encouraged me to overcome the challenges that arose during this process. Last but not least, I also want to thank Alejandra for the constant affection, patience and support with me during this time. Her unconditional disposition and motivation were key to overcome the different challenges and difficulties that appeared during this time.

Abstract

PEÑA UNIGARRO, A.D.**Implementation and simulation of drift-diffusion models for organic mixed conductor devices**. 2022. 84p. Dissertation (Master of science) - Physics Institute of São Carlos, University of São Paulo, São Carlos, 2022.

In the past years, organic electrochemical transistors (OECTs) have emerged as potential transducers in applications that require the conversion of ion fluxes to electronic current. For the rational optimization and understanding of the fundamentals of OECTs and OECT-based applications, however, it is essential to have theoretical models capable to predict experimental data. Within drift-diffusion models, ion flux from the electrolyte into the organic semiconducting layer is considered to take place due to the action of an electrical field, but also because of diffusion processes generated by the concentration gradients. The governing equation of the drift-diffusion model is the Nernst-Planck equation. Thus, in this project, a numerical approach is followed in order to solve the Nernst-Planck equation in one dimension, and model the ion migration from the electrolyte to the semiconductor. To evaluate the accuracy of the implementation, standard boundary conditions used in the literature to solve analytically the drift-diffusion equations were considered. In doing so, the numerical results were in good agreement with the analytical solutions, achieving maximum errors in the order of 1%. Aiming to a better representation of OECTs, closed boundary conditions are considered. Here, the temporal evolution of the concentration profiles showed a convergence to an exponential steady state distribution, which is in good agreement with the result expected theoretically. A further situation investigated was the consideration of a non-uniform electric field acting on the system, assumed to be finite in the electrolyte region and zero in the semiconductor. This consideration impacts principally the temporal evolution of the concentration in each region. In order to consider the distinct compositions in electrolytes and semiconductors, different values of diffusion coefficients were introduced for each region. This extension has visible impacts in the time that the system needs to achieve the steady state. Moreover, the introduction of the chemical potential gradient as the driving force of diffusion leaded to significant variations in the results obtained with the model. Here, the so-called “uphill” diffusion reported in the literature was observed. With the numerical approach, it was possible to consider different types of pulsed gate voltages, which allowed to simulate the charge and discharge processes of OECTs. For all cases, oscillatory curves similar to experimental measurements were obtained. Therefore, the numerical approach allowed to go beyond the analytical description, and develop an extensive investigation of the impact that different considerations have in the results.

Keywords: Finite differences. Organic electronics. Drift-diffusion. OECT.

Resumo

PEÑA UNIGARRO, A.D.**Implementação e simulação de modelos drift-diffusion para dispositivos de condutores orgânicos mistos**. 2022. 84p. Dissertação (Mestrado em Ciências) - Instituto de Física de São Carlos, Universidade de São Paulo, São Carlos, 2022.

Nos últimos anos, os transistores eletroquímicos orgânicos (OECTs) surgiram como transdutores em aplicações que requerem a conversão de fluxos iônicos em corrente eletrônica. Para a otimização e compreensão dos fundamentos das OECTs e suas aplicações, é essencial ter modelos teóricos capazes de prever dados experimentais. Nos modelos de *drift-diffusion*, o fluxo de íons do eletrólito para a camada semicondutora orgânica é considerado como tendo lugar devido à ação de um campo elétrico, mas também devido aos processos de difusão gerados pelos gradientes de concentração. A equação governante do modelo de *drift-diffusion* é a equação de Nernst-Planck. Assim, neste projeto, uma abordagem numérica é seguida para resolver a equação de Nernst-Planck em uma dimensão e modelar a migração iônica do eletrólito para o semicondutor. Para avaliar a precisão da implementação, foram consideradas as condições de contorno padrão utilizadas na literatura para resolver analiticamente as equações de *drift-diffusion*. Ao fazê-lo, os resultados numéricos obtidos mostraram boa concordância com as soluções analíticas, alcançando erros no ordem de 1%. Visando uma melhor representação das OECTs, são consideradas as condições de contorno fechado. Aqui, a evolução temporal dos perfis de concentração mostraram uma convergência para uma distribuição exponencial no estado estacionário, que está em boa concordância com o resultado esperado teoricamente. Adicionalmente, foi considerado um campo elétrico não uniforme atuando sobre o sistema, assumido como finito na região do eletrolito e zero no semicondutor. Esta consideração afeta principalmente a evolução temporal da concentração em cada região. Com o objetivo de considerar as composições distintas em eletrólitos e semicondutores, foram introduzidos diferentes valores de coeficientes de difusão para cada região. Esta extensão tem impactos visíveis no tempo que o sistema precisa para alcançar o estado estacionário. Além disso, a introdução do gradiente do potencial químico como a força responsável da difusão dos íons levou a variações significativas nos resultados obtidos com o modelo. Aqui, a chamada difusão "scendente" relatada na literatura foi observada. Com a abordagem numérica, foi possível considerar diferentes tipos de tensões pulsadas no eletrodo da porta, o que permitiu simular os processos de carga e descarga dos OECTs. Para todos os casos, foram obtidas curvas oscilatórias semelhantes às medidas experimentais. Portanto, a abordagem numérica permitiu ir além da descrição analítica, e desenvolver uma extensa investigação do impacto que diferentes considerações têm nos resultados.

Palavras-chave: Diferenças finitas. Eletrônica orgânica. Drift-diffusion. OECT.

Contents

1 Introduction

1.1 Conducting Polymers

Polymers are organic macromolecules composed by long carbon-chain, formed by monomeric units linked through covalent bonds.[1] Due to their chemical properties, common polymers, such as polyethylene, are normally used in the industry as electrical and thermal insulators.[2] On the other hand, the so-called semiconducting polymers (SCPs) have gained increasing attention, as they represent a good alternative to their inorganic counterparts.[3,4] The key characteristic in SCPs is an alternating single and double bonds in the backbone, which leads to the formation of a delocalized π-system that enables the electronic transport through the material.[1,5] To efficiently increase the electronic transport in these materials, however, the energy gap between the highest occupied molecular orbital (HOMO) and the lowest unoccupied molecular orbital (LUMO) should be reduced. As the polymers can be easily oxidized (or reduced), doping protocols are commonly used to increase the conductivity (σ) by several orders of magnitude.[6] In some cases, the conductivity exceeded the range of semiconductors ($10^{-6}\,\mathrm{S\,m^{-1}} < \sigma < 10^{-2}\,\mathrm{S\,m^{-1}}$), reaching the performance of metallic semiconductors ($10^{2}\,\mathrm{S\,m^{-1}} < \sigma < 10^{8}\,\mathrm{S\,m^{-1}}$).[7,8] Due to the importance of this discovery, Alan MacDiarmid, Hideki Shirakawa and Alan J. Heeger were honored with the Nobel Prize in chemistry in 2000.[9] Since then, the study of SCPs has generated entirely new scientific concepts, as well as the potential for new technologies.

Among the diverse pallet of SCPs, polythiophene and its derivatives are extensively studied for their environmental, thermal stability and overall good processability.[10,11] These materials are widely used for the fabrication of non-linear optical devices, photochromic modules, polymer LEDs, among others.[12–17] The highly stable conductive polycation Poly(3,4-etilenodioxitiophene) (PEDOT) is an important derivative of polythiophene, and it has been studied intensively in the last decades.[18–23] The main problem of this polymer, however, is its insolubility in water. Nevertheless, this was successfully overcome by the addition of the polyanion Poly(estirenosulfonate) (PSS) as a counter ion into the PEDOT matrix.[10] The polymer PEDOT:PSS (see Figure 1.1(a)) present different properties, such as good film forming ability, intrinsically high work function and good physical and chemical stability in air.[23] Further, conductivities from $10^{-2}\,\mathrm{S\,cm^{-1}}$ up to $10^{3}\,\mathrm{S\,cm^{-1}}$ have been reported in the literature,[23] turning PEDOT:PSS in one of the most successfully used materials in terms of practical applications.[23–26] Besides PEDOT:PSS, polymer Poly(3-hexylthiophene) (P3HT) (see Figure 1.1(b)) is another polythiophene derivative with applications focused on its opto-electronic properties. P3HT is also a prototype material among SCPs, due to its wide availability, low production cost, well-known morphology and easy processability.[10,27,28]

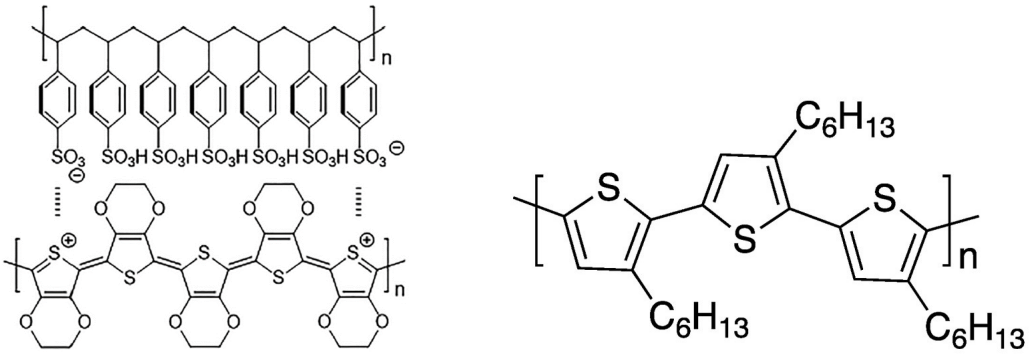

(a) (b)

Figure 1.1 - Chemical structure of (a) PEDOT:PSS and (b) P3HT.
Source: Adapted from GUEYE;[29] JIANG.[30]

1.2 Organic Electronics

The various advances in semiconducting polymers gave rise to a new field of research, named Organic Electronics.[31] This new active subject covers several topics in physics, chemistry, engineering and material science, specifically, materials development, fabrication process, devices design and modeling, device characterization to name a few.[32] Interest in organic electronic materials, and in particular their potential for low-cost fabrication, led to the development of applications widely used today such as Organic Field Effect Transistors (OFETs),[33,34] Organic Solar Cells (OSCs),[27] Organic Light Emitting Diodes (OLEDs),[35] and recently Organic Electrochemical Transistors (OECTs).[36]

The OECTs were developed by Wrighton *et al.*,[37] who presented in the 80s the first organic electrochemical transistor as an alternative to the regular transistors technology existing at that time. After this first seminal paper, OECTs became very popular in academia, being applied as the platform base of numerous applications, *e.g.*, circuit elements,[38] neuromorphic devices,[39] and bioelectronics applications,[24] among others.[38–43] In an OECT, the SCP is in direct contact with an electrolyte, in which an electrode called gate is immersed. Two further electrodes (source and drain) are bridged by the organic semiconductor film, defining the channel, through which electric current flows. The application of a gate voltage generates ion migration from the electrolyte to the semiconductor film, which cause variations in the doping state of the SCP, modifying its conductivity.[44,45] The drain current in the channel between source and drain electrodes depends on the quantity of mobile charge carriers (*i.e.*, holes or electrons), and can be modulated by the voltage applied to the gate (V_G).[36] During OECT operation, two regimes can be identified. On the one hand, the transient response is observed when doping (or de-doping) of the semiconductor material is still in progress (the electrolyte still exchange ions with the polymer bulk). On the other hand, the steady state response occurs when the channel has been completely charged with ions coming from the electrolyte, and the redox processes inside the material no longer takes place.

In order to keep improving the performance of organic electronic devices (and SCPs alike),

however, it is essential to keep exploring and developing new characterization and data processing methods. In terms of modelling efforts, there have been a large number of models seeking to simulate the process occurring inside on a OECT.[46–57] Nevertheless, the rich theory of the ionic-electronic conductivity is still not well understood. Most models available in the literature considers the ion flux coming from the electrolyte to the organic semiconductor simply a consequence of the applied electric field. More recently, several approaches based on drift-diffusion models were suggested, which consider an additional contribution due to the diffusion process. This affects ion motion and consequently the flux created in the electrolyte-channel interface, which is essential to describe the transient behavior of OECTs. In the drift-diffusion based models, the governing equation is the so-called Nernst-Planck equation, for which an analytical solution can be defined under certain conditions. The simplifications needed to analytically solve the drift-diffusion equations, however, usually decrease the generality of the solution, and limit the results to specific cases.[58] Thus, the major aim of this work is to develop a one dimensional numerical model based on drift-diffusion capable of simulate OECTs.

1.3 Objectives & Outline

Considering standard conditions, a numerical approach will be developed in order to solve approximately in one dimension the equations involved in the drift-diffusion model. Since boundary conditions are fundamental to properly represent a realistic device, the implementation of various boundary conditions and their impact on the concentration profile, ion flux at the electrolyte-semiconductor interface and the drain current must be analyzed. As previously mentioned, the conditions assumed to obtain an analytic solution do not always represent a realistic system. Therefore, one objective of this project will be to overcome the limitations of the analytical description, and investigate the impact that additional considerations have in the results. In doing so, challenges like numeric errors and an increase in the computational resources may arise. Thus, it is expected to identify as well the advantages and limitations of the numerical approach.

The objectives of this work can be grouped into four main parts:

1. To formulate and implement a numerical model capable of solving approximately the drift-diffusion equations with minimized errors.

2. To validate the numerical results by comparing them with the analytical solutions reported in the literature.

3. To use the numerical model to investigate situations that go beyond the analytical description.

4. To investigate the viability of numerical solutions and identify the advantages and limitations of this approach.

This work is organized as follows: In the next chapter, the theoretical relevant background is briefly presented. In particular, in Section 2.1 the fundamental considerations of drift and diffusion as well as the equations involved are introduced. Section 2.2 gives an overview on the different models reported in the literature to describe OECTs. In particular, the Bernards-Malliaras model, the Faria-Duong model and the Coppedé model are discussed. Further, in Section 2.3.6 an introduction of numerical methods used to approximate the solution for the partial differential equations are described. Basic concepts of finite differences and numerical approaches are also mentioned in this section.

In Chapter 3, details on the computation and implementation are presented and discussed. Moreover, a brief description of each situation investigated with the model, and the method used to ensure reliable results are presented in this section.

Chapter 4 summarizes the obtained results and their discussions in line with the objectives stated in the Section 1.3. Section 4.1 presents a validation of the implementation by considering standard conditions, for which an analytical solution exist. The accuracy of the numerical solution and the interpretation of the conditions assumed are also analyzed and discussed. In Section 4.2, closed boundary conditions are introduced and its effect in the flux at the interface and the drain current is investigated. Then, in the Section 4.3, Section 4.4, Section 4.5 and Section 4.6, an analysis of the impact on the results when different versions of the model is presented. In particular, the conditions implemented include a non-uniform electric field, different diffusion coefficients in the electrolyte and the semiconductor region, the introduction of the chemical potential and a time dependent gate voltage. Finally, in Chapter 5 the work is summarized and concluded. Moreover, the perspectives for future works are given.

2 Theoretical Background

2.1 Ionic Transport

Diffusion

When particles are suspended in a liquid (or gas), their movement constantly undergo small, random fluctuations due to collisions with the surrounding particles. Such behavior is named Brownian motion in honor to the biologist Robert Brown, the first scientist to study such fluctuations.[59] In a given medium, if a number of particles are subjected to an unbiased Brownian motion, *i.e.*, there is no preferred direction to the random oscillations, over a period of time, the particles will tend to spread evenly throughout that medium.[60,61] In order to understand the random motions inside the system, it would be of interest to study the individual paths of such particles, within a liquid media. The problem, however, is way too complex for a practical solution. Through Newton's laws of motion, for instance, the knowledge of the position and velocity of each of the particles are needed, which in normal situations is very difficult to obtain. Therefore, it is useful to use approaches that allows treating the system macroscopically. In 1855, by analogy with the theory of heat conduction, Adolf Fick described the properties of aqueous diffusion with the formulation of his first law, which is expressed as:[62]

$$\vec{J}_D(r,t) = -D\nabla\psi(r,t)\,, \tag{2.1}$$

where D is the diffusion coefficient and $\psi(r,t)$ is the time dependent concentration. The first Fick's law states, therefore, that the diffusion process is a net migration of particles in the opposite direction of concentration gradient, *i.e.*, they go from regions of higher concentration to regions of lower concentrations (see Figure 2.1). Therefore, diffusion can be considered a macroscopic manifestation of the Brownian motion. In order to ensure the total number of particles conservation, the expression usually named as Fick's second law[62,64] can be introduced,

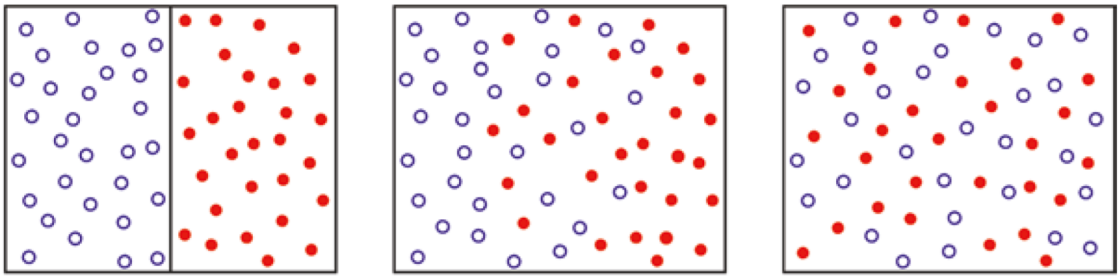

Figure 2.1 - Schematic of diffusion process.
Source: Adapted from KRAUME.[63]

which is expressed as:

$$\left(\frac{\partial \psi}{\partial t}\right) = -\nabla \cdot \vec{J}\,. \tag{2.2}$$

The Fick's laws are the basis for the treatment of many time-dependent transport problems, such as the gas exchange through cell membranes[65] or charge transport inside electrochemical systems,[66] and are normally used to determine diffusion coefficients.[64]

Drift

According to Newton's equation, a particle changes its movement upon an applied force. For instance, in the presence of an electric field, charged species will move in response to the Coulomb force exerted by the field. This drift flux can be expressed as:

$$\vec{J}_E(r,t) = \chi z \mathrm{e} \psi(r,t) \vec{E}(r)\,, \tag{2.3}$$

where χ is the ionic mobility, ψ the ion concentration, z the charge number (or valence) of the specie studied, e the charge of an electron and $\vec{E}$ the field applied. Note that with $\sigma = \chi z e \psi(\vec{r},t)$, Equation (2.3) resamples Ohm's law.

Nernst-Planck Equation

In general, a complete description of the transport of charged particles would have contributions of diffusion and drift factors. In this case, the governing equation is the so-called Nernst-Planck equation,[67,68] which for a charged specie i is given by:

$$\vec{J}_i = J_D^i + J_E^i = -D\nabla\psi_i + \chi z \mathrm{e} \psi_i \vec{E}\,. \tag{2.4}$$

Although Nernst recognized that mobilities and diffusion coefficients present similar properties, it was only until 1905 that an expression relating diffusion coefficient D and ionic mobility χ was established by Albert Einstein.[69] Such expression is given by:

$$D = \chi k_B T^{\mathrm{a}}. \tag{2.5}$$

where k_B is the Boltzmann constant and T^{a} the absolute temperature. In consequence, Equation (2.4) can be written as:

$$\vec{J}_i = J_D^i + J_E^i = -D\nabla\psi_i + \frac{z\mathrm{e}D}{k_B T^{\mathrm{a}}} \psi_i \vec{E}\,. \tag{2.6}$$

In this description, the flux density has contributions from the diffusion processes and the drift due to the electric field. Equation (2.6) along with Fick's second law (see Eq. (2.2)) form a system of nonlinear partial differential equations that compose a set of equations describing the basis of drift-diffusion theory.[53,70,71] The substitution of Eq. (2.6) into Eq. (2.2), leads to

the governing equation for drift-diffusion, which in one dimension is given by:

$$\frac{\partial \psi_i}{\partial t} = D\frac{\partial^2 \psi_i}{\partial x^2} - \beta\frac{\partial}{\partial x}(\psi_i E)\,, \tag{2.7}$$

where the parameter β is defined as

$$\beta = \frac{z\mathrm{e}D}{k_B T^{\mathrm{a}}}. \tag{2.8}$$

Equation (2.7) is a well-known differential equation in the literature, and its analytical solution can be calculated for different initial and boundary conditions.[58]

Chemical potential

In thermodynamics, the chemical potential accounts for the variation in a thermodynamic state function when changes in the number of molecules are produced.[72] Depending on the experimental conditions, the characteristic thermodynamic state function is either Gibbs energy (G), enthalpy (H), Helmholtz energy (A), or the internal energy (U). Thus, for a system with N components, the chemical potential μ_i of a species i may be expressed as:[73]

$$\mu \equiv \left(\frac{\partial G}{\partial n_i}\right)_{T^{\mathrm{a}},p,n_{j\neq i}} = \left(\frac{\partial A}{\partial n_i}\right)_{T^{\mathrm{a}},\nu,n_{j\neq i}} = \left(\frac{\partial U}{\partial n_i}\right)_{s,\nu,n_{j\neq i}} = \left(\frac{\partial H}{\partial n_i}\right)_{S,p,n_{j\neq i}}, \tag{2.9}$$

where n_i is the number of moles of specie i , T^{a} the absolute temperature, P the pressure, S the entropy and ν the volume. Using this description, the changes in the free energy of a system due to addition or subtraction of particles can be investigated. For ideal systems, the chemical potential may be written in function of the concentration as:

$$\mu(x,t) = \mu_0(x) + RT^{\mathrm{a}}\ln(\psi(x,t))\,, \tag{2.10}$$

where μ_0 is the reference or standard chemical potential.[72] In physics, rather than determine the absolute value of a potential, *e.g.*, electrical or gravitational, in a given state, the potential difference in relation to a reference state is measured or calculated. Therefore, the chemical potential is calculated considering μ_0 as the reference value. When pure elements and compounds at $298\,\mathrm{K}$ and $1\,\mathrm{bar}$ are considered, the reference potential can be considered equal to zero.[72]

Initially, in the diffusion theory developed by Fick, it was established that the diffusion flux depends on the concentration gradient.[62] In a more accurate description, however, one should consider that the diffusion processes are driven by the chemical potential gradients instead.[74,75] In such description, the flux of the specie i due to diffusion in one dimension is given by:

$$J_D^i = -B\psi_i\frac{\partial \mu_i}{\partial x}\,, \tag{2.11}$$

where B is a constant related to the mobility of the particles.[72] Thus, the gradient of the chemical potential is known to be the driving force for pure diffusion. Therefore, at equilibrium, *i.e.*,

$J_D^i = 0$, the chemical potential μ_i must achieve a constant value throughout the system. The application of the derivative to the Equation (2.10) leads to:

$$J_D^i = -BRT^{\mathrm{a}} \frac{\partial \psi_i}{\partial x} \, . \tag{2.12}$$

By analogy with the first Fick's law (see Equation (2.1)), it is concluded that $D = BRT^{\mathrm{a}}$. Thus, a relationship between the first Fick's law, and the phenomenological treatment of a transport process is found through a chemical potential formulation. In drift-diffusion case, the one dimensional flux generated for the motion of the charged specie i is given by:

$$J_i = -B\psi_i \frac{\partial \mu_i}{\partial x} + \frac{z\mathrm{e}D}{k_B T^{\mathrm{a}}} \psi_i E \, . \tag{2.13}$$

Using the definitions $R = N_A k_B$, $F = eN_A$ (where N_A is the Avogadro's number), and the relation $D = BRT^{\mathrm{a}}$, Equation (2.13) can be expressed as follows:

$$J_i = -\frac{D}{RT^a} \psi_i \frac{\partial \overline{\mu}_i}{\partial x} \, , \tag{2.14}$$

where $\overline{\mu}_i$ is the electrochemical potential defined as:

$$\overline{\mu}_i(x) = \mu_i(x) + \mathrm{e}FV(x) \, . \tag{2.15}$$

Here, the derivative of the electric potential $V(x)$ defines the electric field applied to the system.

2.2 Organic Electrochemical Transistors

2.2.1 Working mechanism

The invention of the transistor represents an inflection point in the history of the microelectronics. Its optimization and miniaturization led to the integrated circuits, which are actually present in almost every electronic device. With the advancing in the organic electronics, along the researches related to the conducting polymers, different options were developed in order to complement the inorganic components in the transistors. As outlined in the introduction, a transistor is a device in which a current can be modulated via an electrical signal. In an OECT, this modulation is achieved making use of the ability of conjugated polymers to change the electrical conductivity by doping.[5] The typical architecture of an OECT is depicted in Figure 2.2.

In regular OECTs, an organic semiconductor material interconnects two electrodes, which are usually referred to as source and drain. This forms the channel through which an electric current I_D flows once a potential difference V_D is applied between these two contacts. The organic semiconductor is in contact with an electrolyte, in which a third electrode, so-called gate, is immersed. Typically, an electrolyte is a liquid or a viscous gel that possesses mobile ions. Upon an application of a gate voltage (V_G), ions migrate from the electrolyte into the organic

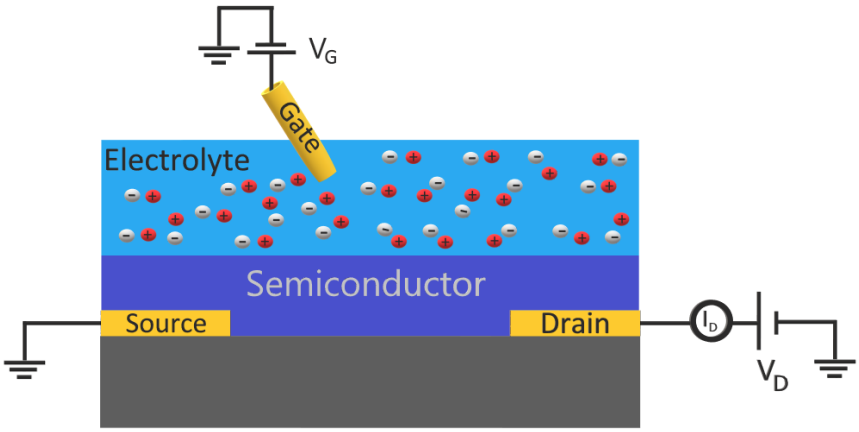

Figure 2.2 - Typical structure of an OECT.
Source: By the author.

material, resulting in variations in the doping state of the conjugated polymer. Consequently, the channel conductivity is changed depending on V_G.

In general, there are two operation modes of OECTs, depending on the initial doping level of the SCP. A pristine conjugated polymer, such as P3HT, for instance, possesses a low conductivity due to its small charge carrier concentration. Upon application of a gate voltage, ions from the electrolyte swells the bulk of the SCP, rising its doping level, yielding an increase in conductivity and consequently an electric current.[76,77] This operation mode of OECTs are refereed to as accumulation mode OECTs.[36] On the other hand, a pre-doped organic semiconductor can also be used. In this case, its doping state is reduced when a gate voltage is applied. One famous representative of such a material is the p-type semiconductor PEDOT:PSS, which is used in many types of organic electronic devices.[18–21,42,43] In this polymer blend, the conjugated polymer PEDOT is in a p-doped state, counter balanced by the negative PSS units (see Figure 1.1(a)). Such an OECT is referred to as depletion mode OECT (Figure 2.3), which due to its wide use, represent one of the most studied types of OECTs.[36] Although the models reported in the literature mostly describe depletion mode OECTs, the theory can be easily extended to

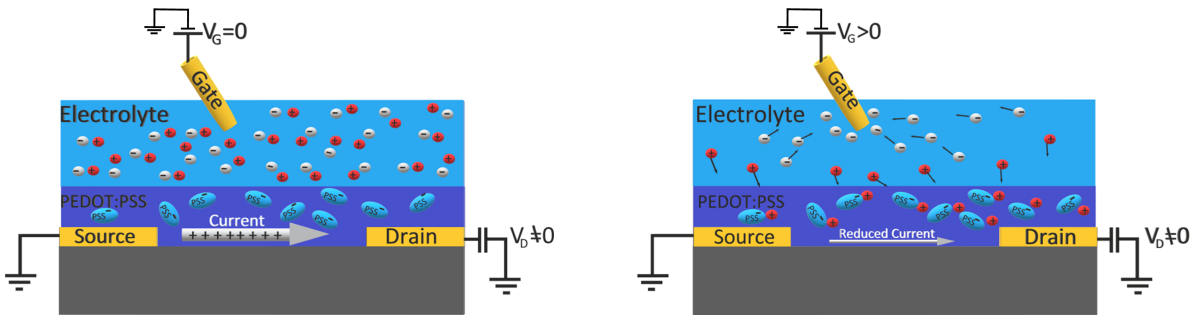

(a) ON state (b) OFF state

Figure 2.3 - Representation of (a) ON and (b) OFF states for an OECT working on depletion mode.
Source: By the author.

the description of devices working in accumulation mode as well.[71] Hence, the focus of this work will be mainly on the description of depletion mode OECTs.

In order to model an OECT, it is meaningful to reduce the spatial degrees of freedom. The simplification to a two-dimensional representation, as depicted in Figure 2.2, is rather straightforward. Nevertheless, describing this scenario remains a complex problem. For this reason, more practical approach have already been discussed in literature, where the problem is further reduced to one dimension.[44,53,54,56,78–80] In 2007, D. Bernards and G. Malliaras[44] reported the first of such formulations, which became the standard capacitive models broadly used to extract device and materials parameters for OECTs in the steady state. Later, G. C. Faria and D. Duong extended the concept introduced by Bernard and Malliaras in order to improve the description of transient behavior of OECTs.[56] Both of these models, however, mostly consider the ion migration due to the applied gate voltage, but do not consider diffusion processes. More refined models, which consider both drift and diffusion processes are recently formulated, especially to describe the transient characteristics of OECTs.[51,53,81] For example, Coppedé *et al.* used an analytical solution of the drift-diffusion equation to obtain a model where the ion diffusion coefficient remained the only unknown parameter. Fitting experimental data with their model, allowed to investigate the impact of different ionic species in the output characteristics of OECTs.[53] Nevertheless, the Coppedé's model is limited by the boundary conditions used to solve analytically the drift-diffusion equation, which do not represent properly an OECT. Although several advances have been developed in the field, the rich nature of the mixed conduction in conjugated polymers is still far from been completely understood. Therefore, further research is needed to articulate design parameters for high performance OECT materials. In the following, the Bernards-Malliaras model, the Faria-Doung model and the Coppedé model will be reviewed in more detail.

2.2.2 Bernards-Malliaras model

Although other device models were previously proposed,[47,48] the Bernards-Malliaras (BM) model was one of the first capacitive models that is largely used up to today for extracting characteristic parameters of OECTs. The starting point of the model is considering Ohm's law[82] to express the current density in the semiconducting channel:

$$J(y) = \sigma \frac{\mathrm{d}V(y)}{\mathrm{d}y} = \mathrm{e}\chi_e \rho \frac{\mathrm{d}V(y)}{\mathrm{d}y} \,. \tag{2.16}$$

Here, σ is the conductivity, e is the elementary charge, χ_e and ρ are the mobility and density of the charge carriers, *i.e.*, holes or electrons, respectively. Moreover, $V(y)$ is the electric potential along the transistor channel.

In a PEDOT:PSS based OECTs, the semiconducting material possesses an intrinsic hole concentration ρ_0. Hence, without gate voltage (V_G), electronic current can flow through the channel. When $V_G > 0$, ions are injected from the electrolyte into the semiconductor volume

ν, compensating the PSS anions in the channel. To maintain the electrical neutrality, the film is de-doped, which means that the holes extracted are not replenished. Therefore, ρ can be expressed in dependence of the total charge Q of cations that migrates from the electrolyte to the channel by the following empirical expression:

$$\rho(Q) = \rho_0(1 - \frac{Q}{\mathrm{e}\rho_0\nu}) \,. \tag{2.17}$$

In the case when $V_G = 0$, meaning that $Q = 0$, Eq. (2.17) yields $\rho = \rho_0$, *i.e.*, the material has its intrinsic conductivity. In the limit when $Q = q\rho_0\nu$, the polymer is fully de-doped and the charge density vanishes. Equation (2.17) can be inserted in Eq. (2.16), leading to:

$$J(y) = \mathrm{e}\chi_e\rho_0(1 - \frac{Q}{\mathrm{e}\rho_0\nu})\frac{\mathrm{d}V(y)}{\mathrm{d}y} \,. \tag{2.18}$$

Steady State

With the aim to find an expression for $Q(V_g)$, the Bernards-Malliaras model divide the semiconductor channel into slices of size $\mathrm{d}y$. This reduces the 2D picture into a simple 1D problem. Each slice is represented by a simple equivalent circuit composed of a resistor R_e and a capacitor C_d in series to describe the ionic contribution of the device properties (see Figure 2.4). The former describes the ionic resistivity of the electrolyte, and the latter is related to the accumulation of charge in the channel. The amount of charge Q of ions entering the channel upon the application of a gate voltage V_g can be estimated by:

$$Q(y) = C_d\Delta V(y) = c_d W T \mathrm{d}y[V_G - V(y)] \,, \tag{2.19}$$

where W is the channel width, T is the film thickness and ΔV is the potential difference between the gate electrode and transistor channel. Further, as the ions are absorbed in the volume, it is more accurate to work with the volumetric capacitance $c_d \equiv C_d/v$.[83]

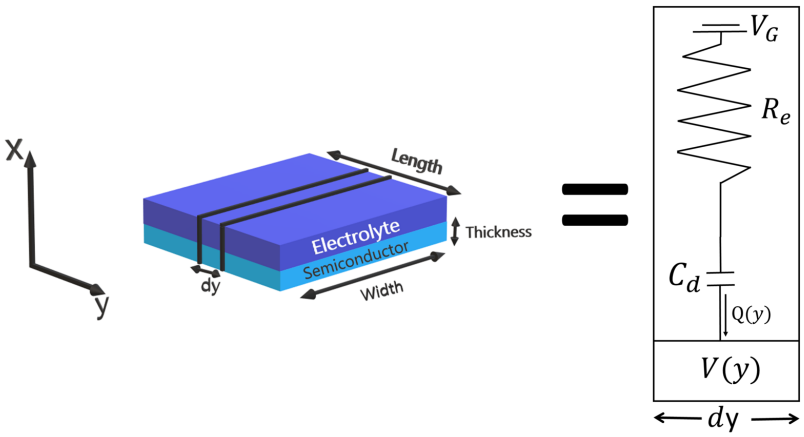

Figure 2.4 - Equivalent circuit considered in the Bernards-Malliaras model.
Source: By the author.

In electrochemical systems, a minimum value of voltage is necessary for oxidation (or reduction) to occur, named as threshold voltage (V_{th}). Bernards and Malliaras did not include this in their model, since V_{th} is very small for PEDOT:PSS, and therefore, negligible. In devices based on other kinds of materials, however, V_{th} might be relevant to consider.[70,71,84] In order to be more general, Equation (2.19) can be extended to:

$$Q(y) = c_d W T \mathrm{d}y[V_G - V_{th} - V(y)] \, . \tag{2.20}$$

Incorporating Eq. (2.20) in Eq. (2.18), the governing equation for the steady-state is obtained as follows:

$$J_{ss}(y) = \mathrm{e}\chi_e\rho_0 \left[1 - \frac{(V_G - V_{th} - V(y))}{V_p}\right] \frac{\mathrm{d}V(y)}{\mathrm{d}y} \, , \tag{2.21}$$

where $V_p \equiv \frac{\mathrm{e}\rho_0}{c_d}$ is the pinch-off potential difference related with the saturation point of the transistor and $V(y)$ the electric potential inside the channel. In order to calculate the current at the steady state I_{ss}, the integration of the Equation (2.21) over the length of the semiconductor is calculated, leading to:

$$I_{ss} = G \left[1 - \frac{(V_G - V_{th} - \frac{1}{2}V_D)}{V_p}\right] V_D \, . \tag{2.22}$$

Here, $G \equiv \frac{WT\mathrm{e}\chi_e\rho_0}{L}$ is the intrinsic conductance of the organic semiconductor film, which accounts for the ability of the material to conduct an electrical current. Equation (2.22) is the Bernards-Malliaras equation for the OECT current operating in the steady state. The expressions derived in BM model has been proven useful for its simplicity, and are commonly used to extract device parameters and to fit device characteristics such as the merit factor $\chi_e c_d$.[85] Nevertheless, the model fails to describe correctly the output characteristics of OECTs, principally due to the square dependence on V_D. The relation obtained for the source-drain current do not lead to a constant current after the saturation. Thus, the equations are only valid until a saturation voltage V_D^{sat} defined by the vertexes of the parabola. Moreover, the model only depends on the geometry of the semiconductor channel, but is completely independent of the nature and characteristic of the electrolyte. Thus, any alteration in the electrolyte will not be reflected in the principal results obtained with the model.

Transient Behavior

When V_G is suddenly changed, the cations migrate from the electrolyte to the semiconductor, and therefore, the channel charge variate as de-doping takes place. This process, however, takes time. The OECT dynamic to reach a new steady state is called transient behavior. Thus, in this situation, time-dependent current contribution associated with doping/de-doping processes must be added to the current, which reflects the extraction of the holes that are not re-injected at the source. For simplicity, in the model, the spatial variation of voltage and hole density within

the channel is neglected. Instead, a correction factor f is introduced to account for the error made when neglecting the spatial variation of the doping/de-doping process.[44] Thus, under these assumptions, the current density is reformulated as:

$$J(t) = \frac{I(t)}{WT} \approx \mathrm{e}\chi_e \rho(t) \frac{V_D}{L} + f\rho L \frac{d\rho(t)}{dt} , \tag{2.23}$$

where $\rho(t)$ is now the temporal dependent charge density and $\frac{V_D}{L}$ the average electric field within the channel. Depending on the magnitude of V_D and V_G, the ion flux coming from the electrolyte into the channel is split between the source and drain electrodes. Normally, the current value captured by the gate electrode defines the factor f, which usually ranges from 0 to $\frac{1}{2}$. In order to calculate the current for the depletion mode case, the Eq. (2.17) is plugged into Eq. (2.23), obtaining:

$$I(t) = I_1 + I_2 = G\left(1 - \frac{Q(t)}{\mathrm{e}\rho_0 \nu}\right) V_D - f\frac{\mathrm{d}Q(t)}{\mathrm{d}t} , \tag{2.24}$$

where, $Q(t)$ the number of ionic charges that the semiconducting channel uptakes over time.

For further developments, the model assumes two independent types of measurements: constant gate current and constant gate voltage. The consideration of a constant gate current leads to $\frac{dQ(t)}{dt} = \frac{Q(t)}{t} = I_G$. This assumption, however, is an oversimplification, which may lead to errors in the model results. Supposing that the transit time is $\tau_e = \frac{L^2}{\chi_e V_D}$, allows replacing V_D in Equation (2.24), leading to:

$$I(t) = I_0 - \chi_e \frac{V_D}{L^2} Q(t) - f I_G = I_0 - t\frac{I_G}{\tau_e} - f I_G , \tag{2.25}$$

where $I_0 \equiv G V_D$ is the initial source-drain current. Bernards and Malliaras applied the Equation (2.25) to constant gate current measurements and were able to extract the transit time τ_e of their material.[44] As discussed early, in the results obtained, intrinsic properties of the device, such as the electrolyte nature and the electric field are not considered. In addition, the model does not fully fit the experimental drain currents nor allows the quantitative extraction of useful device characteristics and ionic impedances.[71]

2.2.3 Faria-Duong model

Equivalent circuits have been extensively used as a helpful tool in electronics to fit currents and impedance responses of a variety of devices. In 2017, G.C. Faria and D. Duong proposed an improvement to the transient Bernards-Malliaras model with the introduction of additional parameters in the equivalent circuit (see Figure 2.5(a)). The so-called Faria-Duong model[56] considers that the drain current $I_D(t)$ can be described as a composition of three contributing currents (see Figure 2.5(b)), thus, I_D may be defined as:

$$I_D(t) = I_0 - f * I_G(t) + \Delta I_{ch} = I_0 - f * I_G(t) \pm g_m V_{ch}(t) . \tag{2.26}$$

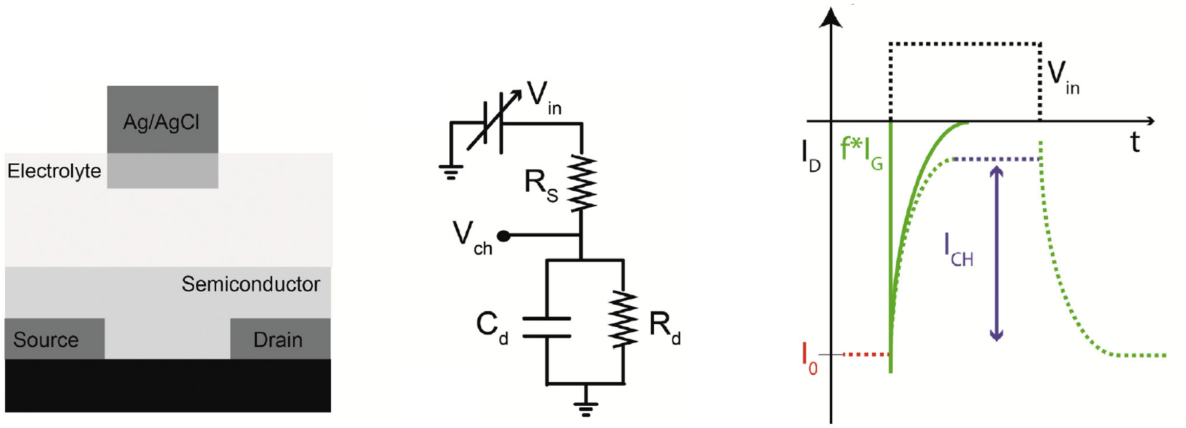

(a) (b)

Figure 2.5 - (a) Equivalent circuit considered in the model. (b) Representation of the three contributing currents composing I_D.

Source: Adapted from FARIA.[56]

In Eq. (2.26), I_0 is the initial drain current before the application of a gate voltage. I_G is the ionic current moving from the gate electrode to the source and drain electrodes. Here, as in the Bernards-Malliaras model, the f factor represents the fraction of ionic current that the drain electrode uptakes. In addition, ΔI_{ch} is the change in the channel current, $g_m = \frac{\partial I_D}{\partial V_G}$ the transconductance and $V_{ch}(t)$ the potential difference in the channel due to the doping/de-doping processes of the active polymer. When a pulse is applied to the gate electrode, an ion flux is generated in the direction of the polymeric film, therefore, creating the current I_G. The Figure 2.5(b) shows the representation of each contribution to the drain current.

For a given device, the values of I_0 and g_m can be obtained experimentally. To determine the parameters $I_G(t)$ and V_{ch}, however, the Faria-Duong model uses an equivalent circuit to represent the OECT. In difference to the Bernards-Malliaras model, the equivalent circuit proposed uses a capacitor C_d in parallel with a resistor R_d. In the model, the capacitor and the resistor are introduced in order to describe the electrolyte-channel interface and the possibility of charge exchange between the ionic specie and the conjugated polymer, respectively. Additionally, a resistor R_s is used to represent the resistance of the electrolytic solution. In their work, the authors use the common approach of circuit analysis based on Laplace transform.[86] Subsequently, impedance circuits composed by time dependent voltages and currents are converted to the frequency domain $\mathbf{s}$. Hence, the problem can be simplified and consequently solved using algebraic manipulations, leading to:

$$
\begin{aligned}
V_{ch} =& \frac{V_0 R_d}{R_d + R_s}\left[1 - \exp(-\frac{R_d + R_s}{C_d R_d R_s}t)\right] \\
I_G =& \frac{V_0}{R_d + R_s} + \frac{V_0 R_d}{R_s(R_d + R_s)}\exp(-\frac{R_d + R_s}{C_d R_d R_s})t \\
I_D =& I_0 + \frac{V_0(g_m R_d - f)}{R_d + R_s} - \frac{V_0 R_d(g_m R_s + f)}{R_s(R_d + R_s)}\exp(-\frac{R_d + R_s}{C_d R_d R_s}t)\,.
\end{aligned}
\tag{2.27}
$$

Here, V_0 is the value of the gate voltage applied. Faria *et al.* used Equation (2.27) to fit the transient response of PEDOT:PSS-based OECT. The model allowed to extract the values of R_s, R_d, C_d, and results useful in the determination of the f factor. Although the model allow to accurately extracting device parameters, some conditions are not considered, *e.g.* the electric field inside the device and the diffusion of ions into the channel.

2.2.4 Coppedé model

The OECT models introduced so far, mostly describe the ion migration from the electrolyte to the semiconductor by capacitive models. The actual process, however, occurs due to the drift and the diffusive movements of ions. Considering a constant electric field E and the same diffusion coefficient D in all regions, the temporal evolution of the concentration is defined by the Nernst-Planck equation (see Section (2.1)), which in one dimension is expressed as:

$$\frac{\partial \psi}{\partial t} = \frac{\partial J}{\partial x} = -D\frac{\partial^2 \psi}{\partial x^2} - D\frac{zeE}{k_B T^{\mathrm{a}}}\frac{\partial \psi}{\partial x} \,. \tag{2.28}$$

Recently, Coppedé *et al.* proposed a one dimensional model (see Figure 2.6(a)) that is based on assuming specific initial and boundary conditions, for which an analytical solution of Eq. (2.28) exists.[58] In particular, the following conditions are considered:

$$\begin{aligned} \psi(x, t=0) &= \psi_0 \; ; \; 0 < x < l \\ \psi(x=0, t) &= 0 \; ; \; t > 0 \\ \psi(\infty, t) &= 0 \; ; \; t > 0 \,, \end{aligned} \tag{2.29}$$

Note that these conditions represent a special case for a more general issue (see Appendix A).

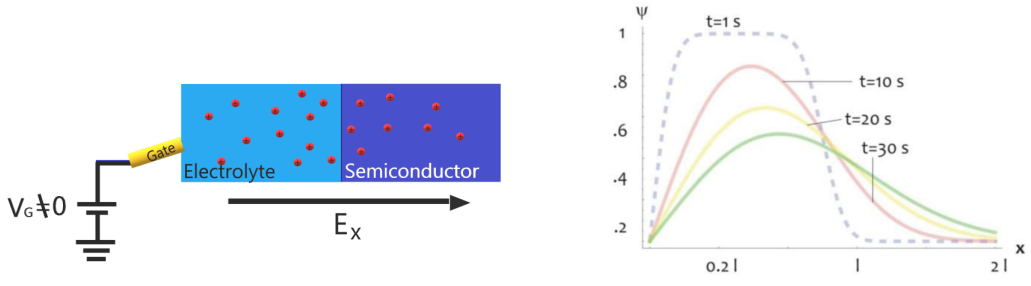

(a) (b)

Figure 2.6 - (a) Schematic of the system considered. (b) Temporal evolution of the concentration in the device. Source: Adapted from COPPEDÉ.[53]

In this situation, the solution is given by:[58]

$$\begin{aligned}\psi(x,t) =& \psi_0(\Upsilon(x,t) - \Omega(x,t)) \\ \Omega(x,t) =& \frac{1}{2}\mathrm{erf}\left[\frac{x-l-\gamma t}{2\sqrt{Dt}}\right] + \frac{1}{2}e^{\gamma x/D}\mathrm{erf}\left[\frac{x+l+\gamma t}{2\sqrt{Dt}}\right] \\ \Upsilon(x,t) =& \frac{1}{2}\mathrm{erf}\left[\frac{x-\gamma t}{2\sqrt{Dt}}\right] + \frac{1}{2}e^{\gamma x/D}\mathrm{erf}\left[\frac{x+\gamma t}{2\sqrt{Dt}}\right] ,\end{aligned} \tag{2.30}$$

$$\mathrm{erf}(t) = \frac{2}{\sqrt{\pi}}\int_0^t e^{-\tau^2}\mathrm{d}\tau \, , \tag{2.31}$$

where l is the electrolyte thickness and $\gamma = \frac{zeD}{k_B T^a}E$. The solution of Eq. (2.28) allow to determine the total amount of charge $Q(t)$ transported into the OECT semiconductor, which is calculated from the flux at the electrolyte-semiconductor interface integrated over time. Therefore, the charge is given by:

$$Q(t) = N_A \mathrm{e} S \int_0^t J(x=l,\tau)\mathrm{d}\tau = N_A \mathrm{e} S \int_0^t \left(\gamma\psi(l,\tau) - D\frac{\partial\psi}{\partial x}|_{x=l}\right)\mathrm{d}\tau \, . \tag{2.32}$$

Here N_A is the Avogrado's number, e the fundamental charge and S the cross-sectional area of the electrolyte. Thus, from the Equation (2.32), it is established the dependence of the charge entering into the semiconductor on the diffusion coefficient. Finally, in order to describe the transient behavior of the drain current, the Bernards-Malliaras assumption is used (see Section (2.2.2)), which is expressed as:

$$I(t) = G\left(1 - \frac{Q(t)}{\mathrm{e}\rho_0\nu}\right)V_D - f\frac{\mathrm{d}Q(t)}{\mathrm{d}t} \, , \tag{2.33}$$

In their work, Coppedé, *et al.* used the model to calculate the density of ions injected into the organic semiconductor (see Figure 2.6(b)). Further, data fitting, allowed them to investigate different ionic species. This model, however, fails in the realistic representation of OECTs. For example, the conditions expressed in Eq. (2.29) describe a situation where the boundaries of the system are defined at the infinity, which is not the case observed experimentally. Additionally, a constant electric field and the same diffusion coefficient in all regions must be taken into account to have a solvable problem. Therefore, the analytical solution presented by Coppedé, *et al.* is only capable of describing specific systems, limited by the considerations mentioned above. Hence, in order to correctly modeling OECTs, additional methods must be implemented.

2.3 Numerical Methods

2.3.1 Partial Differential Equations

When processes in nature are modeled, the mathematical formulation often is expressed by means of partial differential equations (PDEs). In order to define a PDE, let $u = u(x_1, x_2, ..., x_n)$

be a function of n independent variables $x_1, ..., x_n$. A PDE, therefore, is an equation that may contain the independent variables $x_1, ..., x_n$, the unknown function u and its partial derivatives up to some order.[87] In a general form, the PDEs can be expressed as:

$$F(x_1, ..., x_n, u, u_{x_1}, ..., u_{x_n}, u_{x_1x_1}, ..., u_{x_nx_n}) = 0\,, \tag{2.34}$$

where F is a given function and $u_{x_j} = \partial u/\partial x_j$, $u_{x_ix_j} = \partial^2 u/\partial x_i \partial x_j$ $(i, j = 1, ..., n)$ are the partial derivatives of u. The order of PDE is defined by the order of the highest derivative which appears in the equation. To solve the equation, it is necessary to find a function u such that the substitution of u and its derivatives in Equation (2.34) fulfill the identity. Some examples of PDEs used commonly in physics are:

$$u_{tt} - u_{xx} = 0 \text{ (wave equation)} \tag{2.35}$$

$$u_t - u_{xx} = 0 \text{ (diffusion equation)} \tag{2.36}$$

$$u_{xx} + u_{yy} = 0 \text{ (Laplace equation)} \tag{2.37}$$

In order to obtain a unique solution of PDE, a set of supplementary conditions must be provided to determine the arbitrary functions, which results from integration of the PDE.[87,88] The supplementary conditions can be classified as boundary or initial conditions. An initial condition is a requirement for which the dependent variable is specified at some initial state. On the other hand, in boundary conditions, the dependent variable or its derivative must satisfy well-defined requirement on the boundary of the domain of the PDE. Although the boundary conditions used in science and engineering can take various forms, in general can be classified under three types: Dirichlet, Neumann and Robin boundary conditions.[89] If the dependent variable along the boundary is defined, it is known as the Dirichlet type. When the gradient of the dependent variable is specified along the boundary, it is called a Neumann boundary condition. In the case where the condition is composed by a linear combination of the Dirichlet and Neumann types, it is known as the Robin type.

In many cases, defining an analytical solution of the PDEs is not possible. Further, the situations in which it is possible to obtain an analytical result are usually limited by specific conditions, *i.e.*, exist different solutions for different boundary or initial conditions. Therefore, a viable alternative in order to solve PDEs is to use numerical methods. Numerical schemes that are commonly used can be distinguished into three main classes: finite difference (FD) methods, finite volume (FV) methods, and finite element (FE) methods. In the FD methods, the solution domain is represented by a grid. At each grid point or node, the partial derivatives are replaced by approximations in terms of the nodal values of the functions. On the other hand, in the FV and FE methods, the governing equations are integrated over a finite number of volumes or cells. As in this project we shall use the FD method for one dimension, some basic theory of

this approach will be introduced in the following sections.

2.3.2 Grid Generation

The principal idea behind any numerical method is to discretize the domain where the system is considered. In the FD description, the locations at which the variables are going to be calculated are given by a discrete representation (grid) of the region defining the system domain. In this case, the grid points are distributed along grid lines similarly to a Cartesian grid (see Figure 2.7). Depending on the boundary conditions and the functions to be differentiated, uniformly or non-uniformly spaced grid can be used to improve the accuracy of the approximations.

2.3.3 Finite Differences

Finite differences method can be considered to be the oldest approach for numerical solution of PDEs, believed to have been introduced by Euler in the 18th century.[90] In the FD formulation, a relation between the variable value at each node and those at some of the neighboring nodes provide the approximation for the derivative at that point. At the boundary nodes, some conditions need to be defined in order to specify its values. Aiming to understand the idea behind *finite difference* approximation, the derivative of a function f is defined as:

$$\left(\frac{\partial f}{\partial x}\right)_{x=x_i} = \lim_{\Delta x \to 0} \frac{f(x_i + \Delta x) - f(x_i)}{\Delta x} . \tag{2.38}$$

A graphical interpretation of Eq. (2.38) is presented in Figure 2.8 (black dashed line). Therefore, the first derivative $\frac{\partial f}{\partial x}$ evaluated at x_i is the slope of the line tangent to the curve $f(x)$ at that point. In the FD description, three possible approximations for the derivative can be defined, which for an evenly spaced grid are expressed in Eq. (2.39). The *forward difference* approximation calculates the derivative at the point x_i by considering the slope of a line joining the point

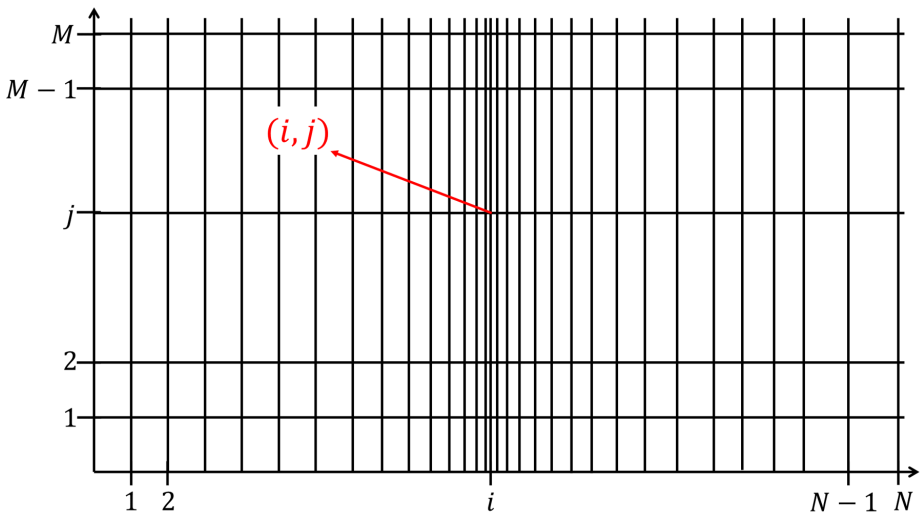

Figure 2.7 - Example for a 2D Cartesian grid for finite differences.
Source: By the author.

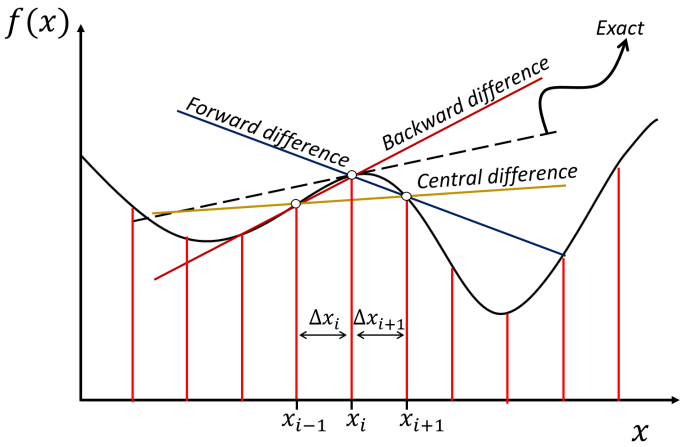

Figure 2.8 - Graphic representation of the derivative and its approximations.
Source: By the author.

x_i and x_{i+1}. If the points x_i and x_{i-1} are considered, the derivative approximation is called *backward difference*. Finally, the *central difference* takes in consideration the points x_{i+1} and x_{i-1}, lying on the opposite sides of the place at which the derivative is approximated. In the Figure 2.8 can be observed that depending on what approximation is being used, the accuracy of the result may change. Further, if an improvement in the quality of the approximation is desired, the grid must be refined, *i.e.* additional points that are closer to each other must be taken into account.[90]

$$\left(\frac{\mathrm{d}f(x_i)}{\mathrm{d}x}\right)_{x=x_i} \approx \begin{cases} \frac{f(x_{i+1})-f(x_i)}{x_{i+1}-x_i} & \textit{Forward Difference} \\ \frac{f(x_i)-f(x_{i-1})}{x_i-x_{i-1}} & \textit{Backward Difference} \\ \frac{f(x_{i+1})-f(x_{i-1})}{x_{i+1}-x_{i-1}} & \textit{Central Difference} \end{cases} \tag{2.39}$$

In this project a non-uniform grid is implemented, therefore, the approximations for the derivatives provided by the FD method use a variable Δx.

2.3.4 First Derivative

Given a continuous differentiable one dimensional function $f(x)$, the Taylor series in the vicinity of x_i can be expressed as:

$$f(x) = f(x_i) + \sum_{n=1}^{\infty} \frac{(x-x_i)^n}{n!} \left(\frac{\mathrm{d}^n f}{\mathrm{d}x^n}\right)_{x=x_i} . \tag{2.40}$$

Making use of the notation $\Delta x_{i+1} = x_{i+1} - x_i$ and $\Delta x_i = x_i - x_{i-1}$ (see Figure 2.8), to calculate the Taylor series for $f(x_i + \Delta x_{i+1})$ and $f(x - \Delta x_i)$ about x_i, the following results are

obtained:

$$f(x_i + \Delta x_{i+1}) = f(x_i) + \sum_{n=1}^{\infty} \frac{(\Delta x_{i+1})^n}{n!} \left(\frac{\mathrm{d}^n f}{\mathrm{d}x^n}\right)_{x=x_i} \tag{2.41}$$

$$f(x_i - \Delta x_i) = f(x_i) + \sum_{n=1}^{\infty} (-1)^n \frac{(\Delta x_i)^n}{n!} \left(\frac{\mathrm{d}^n f}{\mathrm{d}x^n}\right)_{x=x_i} . \tag{2.42}$$

The system composed by Eq. (2.41) and Eq. (2.42) can be solved to obtain an expression for $\frac{\partial f}{\partial x}$. Thus, the first derivative for a non-uniform grid, using *central differences* is defined as:

$$\left(\frac{\mathrm{d}f(x)}{\mathrm{d}x}\right)_{x=x_i} = \frac{f(x_i + \Delta x_{i+1})(\Delta x_i)^2 + f(x_i)[(\Delta x_{i+1})^2 - (\Delta x_i)^2] - f(x_i - \Delta x_i)(\Delta x_{i+1})^2}{(\Delta x_{i+1})(\Delta x_i)[\Delta x_i + \Delta x_{i+1}]} - \frac{\Delta x_{i+1}\Delta x_i}{6} \left(\frac{\mathrm{d}^3 f(x)}{\mathrm{d}x^3}\right)_{x=x_i} + \ldots \tag{2.43}$$

The previous expression is exact if all the terms of the Taylor series on the right side are considered. The higher order derivatives, however, are unknown. As the terms in the expansion depend on the product $\frac{(\Delta x)^n}{n!}\left(\frac{\partial^n f}{\partial x^n}\right)$ $(n = 3, 4 \ldots \infty)$, and Δx is usually a small quantity, the higher order terms will be small if the derivatives of order greater than one are locally small. Therefore, truncating Eq. (2.43) after the first order terms, leads to the approximation of the first derivative as follows:

$$\left(\frac{\mathrm{d}f(x)}{\mathrm{d}x}\right)_{x=x_i} \approx \frac{f(x_i + \Delta x_{i+1})(\Delta x_i)^2 + f(x_i)[(\Delta x_{i+1})^2 - (\Delta x_i)^2] - f(x_i - \Delta x_i)(\Delta x_{i+1})^2}{(\Delta x_{i+1})(\Delta x_i)[\Delta x_i + \Delta x_{i+1}]} . \tag{2.44}$$

For the latest result, two data points are used to define the slope, which are $x_i + \Delta x_{i+1}$ and $x_i - \Delta x_i$. In this case, the approximation possesses a second-order error. If more points are considered, however, a result with a major order of accuracy may be obtained.[90] Further, note that if an evenly spaced grid is implemented, *i.e.* $\Delta x_{i+1} = \Delta x_i$, Eq. (2.44) reduces to the central difference relation expressed in Eq. (2.39).

2.3.5 Second Order Derivative

Many of the governing equations that describe physical processes like the heat equation, or the wave equation involve second order partial derivatives. Therefore, aiming to find an expression for the second order derivative, the Eq. (2.41) and Eq. (2.42) are used again. This time, the system must be solved for $\frac{\partial^2 f}{\partial x^2}$. Thus, the second derivative is expressed as:

$$\left(\frac{\mathrm{d}^2 f(x)}{\mathrm{d}x^2}\right)_{x=x_i} = \frac{f(x_i + \Delta x_{i+1})(\Delta x_i) - f(x_i)(\Delta x_{i+1} - \Delta x_i) + f(x_i - \Delta x_i)(\Delta x_{i+1})}{\frac{1}{2}(\Delta x_{i+1})(\Delta x_i)[(\Delta x_{i+1}) + (\Delta x_i)]} - \frac{\Delta x_{i+1} - \Delta x_i}{3} \left(\frac{\mathrm{d}^3 f(x)}{\mathrm{d}x^3}\right)_{x=x_i} + \ldots \tag{2.45}$$

The leading truncation error in this case is first order, but vanishes when the spacing between the points is uniform ($\Delta x_{i+1} = \Delta x_i$), turning, in this case, to a second-order accurate approximation.[90] By doing a truncation of the series, the approximation of the second order derivative using *central difference* approximation is:

$$\left(\frac{\mathrm{d}^2 f(x)}{\mathrm{d}x^2}\right)_{x=x_i} \approx \frac{f(x_i+\Delta x_{i+1})(\Delta x_i) - f(x_i)(\Delta x_{i+1}-\Delta x_i) + f(x_i-\Delta x_i)(\Delta x_{i+1})}{\frac{1}{2}(\Delta x_{i+1})(\Delta x_i)[(\Delta x_{i+1})+(\Delta x_i)]} \,. \tag{2.46}$$

Therefore, Eq. (2.44) and Eq. (2.46) provide the first and second derivative for the inner points of the domain respectively. For the grid points located at the boundaries, additional boundary conditions must be introduced in order to establish their values.

2.3.6 Numerical method to Solve PDEs

Various techniques can be used to solve the PDE that describes drift-diffusion processes. The model developed in this work, however, is based on the so-called explicit method. Therefore, it is appropriate to introduce and define the general aspects of this approach. In order to approximate a solution for the Nernst-Planck equation (see Eq. (2.7)), different approximations for spatial and temporal derivatives are used. Here, the derivatives calculated for the points of the spatial domain will be approximated using the *central difference* expressions derived previously. As mentioned earlier, in order to guarantee the correct representation of the system, additional conditions must be imposed for the points located at the boundaries. On the other hand, although exists several methods to evaluate approximately the temporal derivative, the computational efforts needed to develop the calculation may increase, leading to larges times to obtain a solution. Thus, results convenient to use the *forward difference* approximation (see Eq. (2.39)) for temporal derivatives. Hence, when a constant electric field E is considered, Eq. (2.7) can be approximated using finite differences as:

$$\begin{aligned}\frac{\psi_i^{j+1}-\psi_i^j}{\Delta t} =& D\frac{\psi_{i+1}^j(\Delta x_i) - \psi_i^j(\Delta x_{i+1}-\Delta x_i) + \psi_{i-1}^j(\Delta x_{i+1})}{\frac{1}{2}(\Delta x_{i+1})(\Delta x_i)[(\Delta x_{i+1})+(\Delta x_i)]} \\ &- \gamma\frac{\psi_{i+1}^j(\Delta x_i)^2 + \psi_i^j[(\Delta x_{i+1})^2-(\Delta x_i)^2] - \psi_{i-1}^j(\Delta x_{i+1})^2}{(\Delta x_{i+1})(\Delta x_i)[\Delta x_i+\Delta x_{i+1}]} \,.\end{aligned} \tag{2.47}$$

Here, $\gamma = \frac{zeD}{k_B T^a}E$, and the notation ψ_i^j is used to refer the concentration $\psi(x_i, t_j)$ at the grid point x_i and time t_j ($i = 1, 2, ..., N_x; j = 0, 1, 2, ...N_t$). Equation (2.47) can be solved for the unknown ψ_i^{j+1}, leading to:

$$\psi_i^{j+1} = \eta_i\psi_{i+1}^j + \alpha_i\psi_i^j + \lambda_i\psi_{i-1}^j \,, \tag{2.48}$$

where η_i,α_i and λ_i are parameters composed of D, γ, Δx_i, Δx_{i+1} and Δt. Note that in the system represented by Eq. (2.48) there is one equation for each grid point x_i. Besides, the concentration ψ_i^{j+1} defined at time t_{j+1} is calculated from the previous solution ψ_i^j, *i.e.* the solution at any time is calculated directly from the concentration at the previous time step. To start the

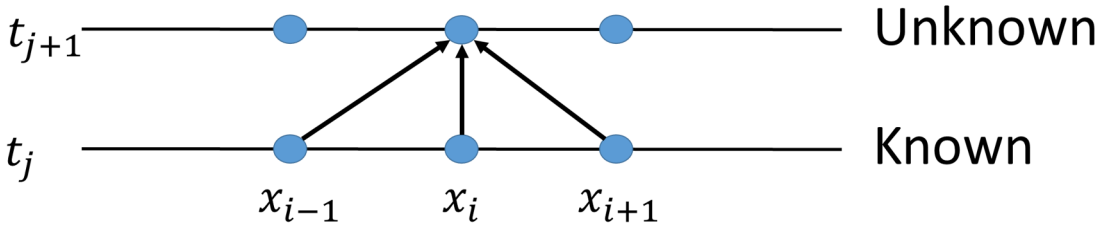

Figure 2.9 - Representation of the explicit method.
Source: By the author.

solution, therefore, an initial condition must be specified. When a problem approximated by finite difference expresses the unknown in terms of the known values, it is defined as explicit method (see Figure 2.9).

Equation (2.48) can be written in matrix notation as follows:

$$\begin{pmatrix} \psi_1^{j+1} \\ \psi_2^{j+1} \\ . \\ . \\ . \\ \psi_{N_x-2}^{j+1} \\ \psi_{N_x-1}^{j+1} \end{pmatrix} = \begin{pmatrix} \eta_1 & \alpha_1 & \lambda_1 & 0 & 0 & . & . & . & 0 & 0 \\ 0 & \eta_2 & \alpha_2 & \lambda_2 & 0 & 0 & . & . & . & 0 \\ & & & & & . & & & & \\ & & & & & & . & & & \\ & & & & & & & . & & \\ 0 & . & . & . & 0 & 0 & \eta_{N_x-2} & \alpha_{N_x-2} & \lambda_{N_x-2} & 0 \\ 0 & 0 & . & . & . & 0 & 0 & \eta_{N_x-1} & \alpha_{N_x-1} & \lambda_{N_x-1} \end{pmatrix} \begin{pmatrix} \psi_1^j \\ \psi_2^j \\ . \\ . \\ . \\ \psi_{N_x-2}^j \\ \psi_{N_x-1}^j \end{pmatrix} \tag{2.49}$$

which in an abbreviated form will be:

$$s^{j+1} = As^j \, . \tag{2.50}$$

Here, the vector s_i^j represents the concentration at time t_j. The values of ψ_0 and ψ_{N_x} that represent the solution at the left and right boundary, respectively, are given at any time by the boundary conditions imposed. In difference with Eq. (2.48) where scalar products and additions have to be calculated to obtain the solution at each point x_i, Eq. (2.50) allow estimate ψ^{j+1} with a single matrix multiplication. As computationally is more efficient to develop matrix operations, expressing the problems as Eq. (2.50), optimizes the computational calculations and reduce the time needed to obtain the solution.

It is important to mention that numerical solutions of the PDEs are only approximated solutions. Therefore, the results obtained numerically may be affected due to errors related to discretization or those that might be introduced in the course of development of the solution algorithm. Moreover, numerical implementations should have certain properties such as stability,[91] which ensures that the solution method does not magnify the errors of the implementation. In general, many solutions schemes require the time step be smaller than a certain limit, which means that the value of Δt is not an independent, arbitrary choice. The parameter Δt, therefore, is restricted to be equal to or less than a certain value prescribed by a stability criterion.[91] If

Δt takes values larger than the limit imposed by the stability condition, the calculations will quickly go unstable, obtaining results such as infinity values. For problems influenced by the boundary conditions, however, the stability is usually difficult to demonstrate. Thus, in order to have a qualitative idea of the stability condition for the numerical implementation developed in this work, the stability criterion for a pure diffusion process considering a uniform grid is investigated in Appendix B. Here, the values of Δt are found to be dependent on Δx and the diffusion coefficient D.

3 Numerical model

As mentioned in Section 2.1, the analytical solution of the drift-diffusion equations have significant limitations associated to the boundary conditions. Furthermore, to define a solution in various situations, such as, non-uniform electric field, non-constant diffusion coefficient, time dependent gate voltage, among others, is not possible. Therefore, exploring the numerical approach to overcome the previously mentioned limitations represent a viable alternative for solving the differential equations involved in the OECT problem. In the following sections, a description of the model developed in this work will be discussed.

3.1 Grid generation

In Section 2.3, it was discussed that the error arising from finite difference approximation depends on the product of $\Delta x \left(\frac{\partial^n f}{\partial x^n}\right)$. Consequently, for a given Δx, it is obvious that for larger values of the derivatives, the error increases proportionally. Using this as motivation, non-uniform grids, *i.e.*, variable Δx, are used for the numeric approximations. Aiming to develop a non-uniform grid with total number of points N_x, an expression composed by a linear (f_{linear}) and a sigmoid function (f_{sig}) is used. This relation is expressed as follows:

$$f_{grid}(i) = f_{linear}(i) + f_{sig}(i) = mi + \frac{A}{1 + e^{-ci}}\,, \tag{3.1}$$

where $i = 1, 2, ..., N_x$, m is the slope of the linear function and the constants A and c represent the amplitude and the width of the sigmoid curve, respectively.

As presented in Figure 3.1(a), f_{grid} can be used to define the spatial domain representing the OECT device, in which the electrolyte and semiconductor thickness has the value T_e and T_{sc}, respectively. In this case, the set of grid points $\{x_0, x_1, ..., x_{300}\}$ represents the system domain, and each value of $x_i = f(i)$ $(i = 0, 1, ..., 300)$ is given by Equation (3.1). Further, the electrolyte-semiconductor interface is considered to be located at the grid point identified with

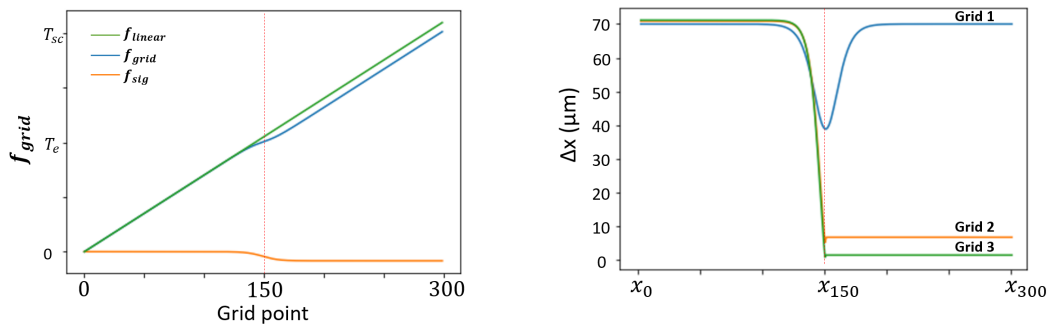

(a) (b)

Figure 3.1 - (a) Grid used in the simulation. (b) Values of Δx for three grids considered in the simulations. Grid 1, Grid 2 and Grid 3 consider $T_{sc} = 1\,\text{cm}$, $T_{sc} = 0.1\,\text{cm}$ and $T_{sc} = 0.01\,\text{cm}$, respectively

Source: By the author.

the index $i = 150$. Note from Fig. 3.1(a) that f_{grid} has a slower increase in its values around the interface ($i = 150$), *i.e.*, more points are considered in this region. This is clearly visible in Figure 3.1(b), where the values of Δx for three different grids are presented. Here, the grid 1, grid 2 and grid 3 refers to the cases in which the semiconductor thickness has a value of $T_{sc} = 1\,\mathrm{cm}$, $T_{sc} = 0.1\,\mathrm{cm}$ and $T_{sc} = 0.03\,\mathrm{cm}$, respectively. As observed in Figure 3.1(b), the three grids are generated to have the minimum value of Δx at the electrolyte-semiconductor interface, where it is expected to have large values of the derivatives. By doing so, the error is compensated. One may use, however, an evenly spaced grid considering the minimum value of Δx, and reduce the error arising from $\Delta x \left(\frac{\partial^n f}{\partial x^n}\right)$ for all region. Nevertheless, in order to obtain smaller values of Δx, more grid points have to be introduced. From the result expressed in Eq. (2.48), it was discussed that for each grid point, exist one equation to be solved. Thus, if more nodes are introduced, the number of calculations that have to be performed increases, which leads to a growth in computational resources needed to obtain the solution. Therefore, the implementation of this grid, allow us to compensate the error arising due to the large derivatives at the electrolyte-semiconductor interface, but maintaining affordable computational times.

As discussed in Section 2.3.6, the value of Δt that has to be used to obtain stable solutions is not arbitrary. Rather, it may depend on the value of Δx_i and the diffusion coefficient D (see Appendix B). For the numerical model developed in this work, $\Delta t = 10^{-3}\,\mathrm{s}$ is the maximum value for which a stable solution is obtained. To improve the accuracy in the temporal derivative, however, a value of $\Delta t = 10^{-5}\,\mathrm{s}$ is used in the simulations.

3.2 Flux and drain current calculation

Typical characterization of OECTs usually involves the experimental measurements of drain current I_D that flows between source and drain electrodes. Therefore, in order to properly simulate these devices, it is important to develop a study on the time evolution of the drain current. Initially, in order to calculate the values of I_D as a function of time, the one dimensional flux at the electrolyte-semiconductor interface located at $x = T_e$, has to be determined. According to Fick's second law (see Section (2.1)), the relation between temporal derivative of concentration and the flux gradient is given by Equation (2.2). Thus, considering a one dimensional system, if forward difference approximation (see Eq. (2.39)) for temporal derivative is used, the integration of Eq. (2.2), leads to:

$$\int_0^{T_e} \left(\frac{\partial \psi(x,t)}{\partial t}\right) \mathrm{d}x = -\int_0^{T_e} \left(\frac{\partial J(x,t)}{\partial x}\right) \mathrm{d}x \rightarrow \int_0^{T_e} \left(\frac{\psi^{j+1} - \psi^j}{\Delta t}\right) \mathrm{d}x = -J(x = T_e, t) + J(x = 0, t)\,. \tag{3.2}$$

As for the situations treated in this work, the flux at the initial position $J(0,t) = 0$, the flux at the interface can be expressed as:

$$J_x(x = T_e, t) = -\int_0^{T_e} \left(\frac{\psi^{j+1} - \psi^j}{\Delta t}\right) \mathrm{d}x\,. \tag{3.3}$$

The flux of ions towards the channel produce changes in the doping state of the material,

creating a transient current I_D. Therefore, in order to describe the transient behavior of OECTs, the Bernards-Malliaras assumption is used to calculate the values of I_D (see Section (2.2.2)).

3.3 Boundary Conditions

Usually, the conditions for which an analytical solution exists, do not always simulate the scenarios observed experimentally. For example, one of the various limitations of the analytic solution for the drift-diffusion model used in the work of Coppedé[53] is related to the boundary conditions (see Section (2.2.4)). In one hand, the situation $\psi(x = 0, t) = 0$ is not necessarily true for real devices, since the concentration, at least in the first time intervals, is distributed in all the electrolyte region. On the other hand, the condition $\psi(x = \infty, t) = 0$ establish a boundary located at the infinity, *i.e.*, the concentration can spread along an infinite system. In a real device, however, a well-defined boundary given by the substrate is the case. Therefore, aiming to improve the representation of OECTs using the drift-diffusion model, the implementation of closed boundaries is investigated. These conditions are based on the assumption of zero flux at the boundaries, and can be expressed as follows:

$$\begin{aligned} J(x = 0, t) &= 0 \\ J(x = T, t) &= 0 \, . \end{aligned} \tag{3.4}$$

Here, T is the total thickness of the system (electrolyte and semiconductor) considered. The implementation of the previous conditions in the Nernst-Planck equation (see Section (2.28)) in one dimension leads to:

$$\frac{\partial \psi(x,t)}{\partial x}|_{x=0,\,T} = \frac{ze}{k_B T} E(x)\psi(x,t)|_{x=0,\,T} \, , \tag{3.5}$$

which establish a relation for the derivative of the concentration at the boundaries. If finite differences (see Section 2.3.6) are used to express the derivative in the previous result, the grid points located at the boundaries can be defined. In Figure 3.2 a schematic of the described device is shown.

(a) (b)

Figure 3.2 - Schematics of the system with closed boundaries considered in the cases: (a) $V_G = 0$ and (b) $V_G \neq 0$. Source: By the author.

3.4 Non-uniform electric field

Due to the mixed conductive property of PEDOT:PSS,[92] the electronic charge carriers within the material react to any electric field applied to the semiconducting film. Following the Born–Oppenheimer approximation,[93] the movement of electronic charge carriers is much faster than the diffusion motion of ions. In consequence, the electronic charges quickly rearrange to compensate the electric field, and at any given time, the electronic distribution is immediately equilibrated. Therefore, as the electric field is given by $E = \frac{\mathrm{d}V}{\mathrm{d}x}$, to have a null electric field within the semiconductor film, the electric potential $V(x)$ must be constant in this region, (Figure 3.3), *i.e.* inside the semiconductor, the ions will move freely, and their motion will be characterized only due to diffusion processes.[46,81] Considering a non-uniform electric field, the Nernst-Planck equation in one dimension turns into:

$$\frac{\partial \psi(x)}{\partial t} = D\frac{\partial^2 \psi(x)}{\partial x^2} - \beta E(x)\frac{\partial \psi(x)}{\partial x} - \beta \psi(x)\frac{\partial E(x)}{\partial x}\,, \tag{3.6}$$

where $\beta = \frac{zeD}{k_B T^{\mathrm{a}}}$ and the electric potential is now given by

$$V(x) = \begin{cases} V_e(x) & if \quad 0 \leq x \leq T_e \\ \\ V_{sc}(x) & if \quad T_e < x \leq T_{sc} \end{cases}\,. \tag{3.7}$$

Here, T_e and T_{sc} represent the thickness of the electrolyte and semiconductor, respectively. When a non-uniform electric field is added into the model, however, several problems arise in the numerical implementation. As in the interface, the finite difference approximation of the derivative may consider the last value of V_e and the first one of V_{sc} (see Eq. (2.44)), the estimation of $E = \frac{\mathrm{d}V}{\mathrm{d}x}$ lead to indeterminacies in this region. In consequence, the temporal evolution of the concentration given by Eq. (3.6) is not well-defined at this point, which means that information of the concentration at the interface is being lost on each time step. Aiming to solve

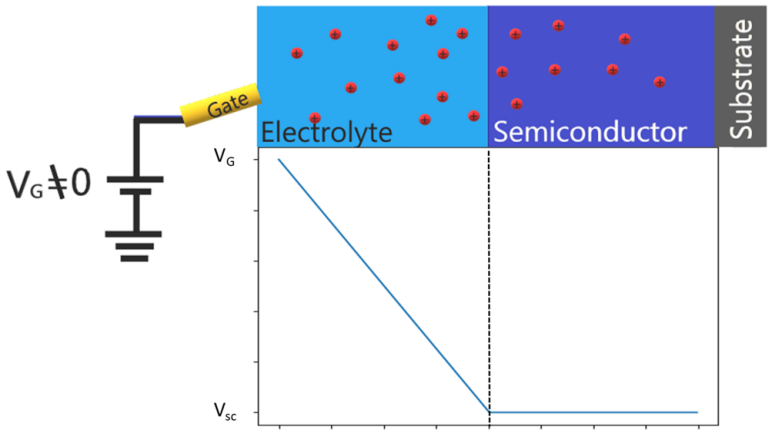

Figure 3.3 - Gate Voltage considered.
Source: By the author.

this problem, the addition by hand of the undefined interfacial contribution of the concentration is proposed. To calculate the contribution of the concentration at the interface, the conservation of the total number of particles is used as motivation. Since the particles entering the semiconductor must be the same as those leaving the electrolyte, if any concentration suffers from an error (systematic or numerical), it will be reflected in the difference between the flux at the interface. Then, once the quantity of missing concentration was determined, the concentration profile can be corrected to fulfill the conservation criterion of total concentration. This correction can be implemented in various form, *e.g.*, evenly in all the points, in the first grid point in the semiconductor region, etc. It is important to mention, however, that each approach will have an impact on the time-evolution of the concentration profile, and consequently on all further derived quantities. As we are assuming an electric field acting only in the electrolyte, we propose the missing concentration ψ_m as a unique contribution located at the interface ($x = x_{int}$), which diffuse towards the semiconductor region. In order to implement this assumption, the value of concentration calculated was distributed on a Gaussian function centered at $x = x_{int}$, which is subsequently added to the semiconductor region. The choice of the Gaussian function is motivated to the fact that this type of function is solution for the second Fick's law (see Appendix C), which describes the temporal evolution of diffusion processes (see Section 2.1). This solution is expressed as:

$$\psi_m = A\exp(-\frac{(x - x_{int})^2}{4D\Delta t}) \,, \tag{3.8}$$

where A is a normalization factor. It is observed that the width Γ of ψ_m is given by $\Gamma = 4\sqrt{D\Delta t}$.[94] Therefore, as Γ is proportional to the square root of Δt, if $\Delta t \to 0$, the whole concentration ψ_m is at the interface. In this way, the system was ensured to conserve the concentration without loosing information at the electrolyte-semiconductor interface.

3.5 Materials properties and OECT characterization

Usually, the electrolyte and the semiconductor have different properties, like morphology and structure. Therefore, intrinsic characteristics such as diffusion coefficient and the electrochemical potential may have different values for each region. Therefore, the situation where the two regions possess different diffusion coefficients is studied. As the diffusion coefficient describes how ease the particles can move inside a material, the implementation of this extension may provide insights about on which region has the most influence on device functioning. Considering the chemical potential as the driving force for diffusion, the flux coming from the electrolyte will be estimated from Eq. (2.14). In order to reflect the distinct compositions of these two materials, different values for the reference chemical potential μ_0 will be considered for each region.

Usually, in order to investigate the charge and discharge properties of an OECT, a pulsed gate voltage is applied to the device. Therefore, in the numerical implementation is investigated

the case in which a time dependent gate voltage is applied. Further, the numerical model allows implementing various shapes of gate voltage and identify the impact of each one in the results.

3.6 Parameters and computational resources

The algorithm used to obtain the solutions was not parallelized, which means that the code runs on a single CPU instead of spreading the work across multiple CPUs.

The different constant used in the simulations are deposited in Table 3.1. For the diffusion coefficient, a value that allowed results to be obtained in viable times and that was close to the typical diffusion coefficients for aqueous solutions reported in the literature[95,96] was used. As previously mentioned, this work is focused on the study of OECTs working on depletion mode, thus, the values for hole concentration and hole mobility used are based in the information reported in the literature for PEDOT:PSS.[44]

Table 3.1 - Constants used in the simulations.

Constants		
Concentration	ψ_0	1 mMol
Diffusion Coefficient	D	$5 \times 10^{-3}\,\mathrm{cm^2 s^{-1}}$
Electrolyte Thickness	T_e	$1\,\mathrm{cm}$
Semiconductor Length	L	$0.1\,\mathrm{cm}$
Semiconductor Width	W	$0.02\,\mathrm{cm}$
Hole mobility	χ_e	$10^{-3}\,\mathrm{m^2 V^{-1} s^{-1}}$
Drain Voltage	V_D	$-0.1\,\mathrm{V}$
Absolute Temperature	T^a	$298\,\mathrm{K}$
Initial Hole concentration	ρ_0	$10^{20}\,\mathrm{cm^{-3}}$

Source: By the author.

In consideration with the minimum values of Δx obtained with the grids implemented, a value $\Delta t = 10^{-5}\,\mathrm{s}$ is used in the simulations. Using these constants, the calculations for a device operating for $1500\,\mathrm{s}$ were performed over a range of 20-24 h. Additional relevant parameters treated in the simulations are inserted in Table 3.2. In particular, T_e,T_{sc} were considered according to the values used in Coppedé's model.[53]

Table 3.2 - Parameters of the simulations.

Simulation Parameteres		
Semiconductor Thickness	T_sc	$0.03\,\mathrm{cm} < T_\mathrm{sc} < 1\,\mathrm{cm}$
Time step	Δt	$10^{-5}\,\mathrm{s}$
Gate Voltage	V_G	$0 < V_G < 100\,\mathrm{mV}$

Source: By the author.

4 Results

4.1 Validation of Numerical Implementation

In order to evaluate the performance and the accuracy of the numerical model and its implementation, a comparison to the analytical model suggested by Coppedé[53] is now considered (see Section 2.2.4). To do so, the same initial and boundary conditions are used, for which the analytical solution (see Eq. (2.30)) of the Drift-diffusion equation holds. These are in particular $\psi(x = 0, t) = 0$ and $\psi(x = \infty, t) = 0$, a constant electric field at all locations x (with strength of $E = 5\,\mathrm{mV\,cm^{-1}}$) and the same diffusion coefficient D for both regions, electrolyte and semiconductor. Moreover, it is assumed a constant concentration of particles (of amplitude ψ_0) in the electrolyte and no initial concentration in the semiconductor (Eq. (2.29)). Further parameters that are relevant to the simulation are summarized in Table 3.1 and Table 3.2.

Figure 4.1(a) displays the temporal evolution of the concentration profile $\psi(x)$. Within the first 10 sec, the initial square-shaped profile turns into an asymmetric bell-shaped form. Due to the drift, the maximum of the distribution moves in the direction of the electric field, whereas simultaneously, the profile broadens because of the diffusion phenomena. As in Coppedé's work,[53] in this section it is also considered the spatial domain of the device defined by $0 < x < 2\,\mathrm{cm}$. Note that over time, the total amount of concentration within the region considered converges to zero. This is a consequence of the boundary condition at the right-hand side ($\psi(x = \infty, t) = 0$), which suggest that the concentration can spread along a system with infinite thickness, *i.e.*, a non-zero flux at $x = 2\,\mathrm{cm}$ is generated. Comparing the distribution obtained numerically with that from the analytical solution, a qualitative good agreement is observed for all times. Especially, the height and lateral position of the maximum as well as the overall shape match very well.

In order to study the accuracy of the numerical implementation quantitatively, the mean

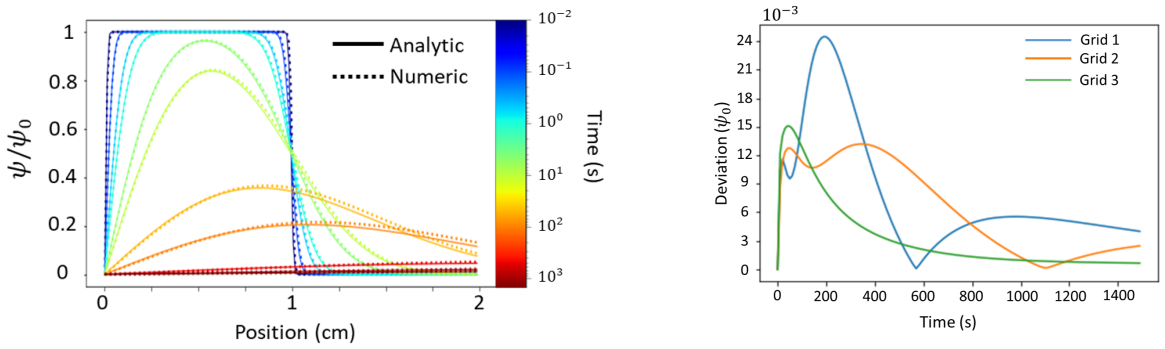

(a) (b)

Figure 4.1 - (a) Time evolution of analytical[53] and numerical solutions. (b) Evolution of the deviation for grid 1 ($0 < x < 2\,\mathrm{cm}$), grid 2 ($0 < x < 3\,\mathrm{cm}$) and grid 3 ($0 < x < 6\,\mathrm{cm}$).

Source: By the author.

deviation (ς) of the numerically obtained concentration profile ψ^{n} in relation to the analytical solution ψ^{a} at the positions x_i defined by the grid, is calculated. For this purpose, the following expression is used:

$$\varsigma = \sqrt{\frac{1}{N_x}\sum_{i=1}^{N_x}\left(\psi^{\mathrm{a}}(x_i) - \psi^{\mathrm{n}}(x_i)\right)^2}\,. \tag{4.1}$$

Figure 4.1(b) shows how ς develops with increasing simulation time t when a grid only defined for $0 < x < 2\,\mathrm{cm}$ (blue line) is considered. For small times ($t < 10\,\mathrm{s}$) as well as for long times ($t > 1000\,\mathrm{s}$), values of ς smaller than $9 \times 10^{-3}\psi_0$ are obtained. For $t < 10\,\mathrm{s}$, the time is not enough to produce significant changes in the initial concentration, thus, the analytical and numerical solutions are identical, leading to small values of ς. As observed from Figure 4.1(a), for larger times ($t > 1000\,\mathrm{s}$), the solutions and consequently ς converge to zero. In between, however, the deviation shows three maxima at about $t = 20\,\mathrm{s}$, $t = 300\,\mathrm{s}$ and $t = 1000\,\mathrm{s}$. The first one is associated to the numerical error that arises from the approximation of the derivative at the interface for the given initial conditions. In the numerical representation, a sudden drop from ψ_0 to 0 take place over a finite spacing defined by the grid. Therefore, the derivative approximations defined in Section 2.3, remains finite, and consequently, generates large errors. This artifact, as mentioned in Section 3.1, is reduced by using a denser grid in the interface region. The second and third maximum of the deviation, on the other hand, arise due to the larger inaccuracy of the numerical approximation of the derivate at the point located at the right boundary. For this point, only the backward difference instead of the central difference method (see Eq. (2.39)) must be used. Hence, as soon as the numerical solution reaches points near $x = 2\,\mathrm{cm}$, this error occurs and propagates into the whole region. In the time between the second and third maxima, ς present a value close to zero, which occurs due to the transition from an overestimation to an underestimation of the numerical result in relation to the analytical solution. This contribution to ς, however, can easily be reduced by extending the simulation region to larger locations. As shown in Figure 4.1(b), the second maximum of ς shifts to larger times and is reduced in height when the simulation grid is extended to $3\,\mathrm{cm}$ (orange line). When the grid is extended further (green line), the second maximum disappears, since the concentration vanishes before the maximum reaches the out-most point at the right-hand side. The calculation of ς represents an estimation of the error distribution between the two solutions. Therefore, considering the absolute values of ς compared to the values of ψ_0, it is found that the numerical implementation yields quite small error. In particular, when a grid defined for $0 < x < 6\,\mathrm{cm}$ is used, maximum values of ς in the order of $\sim 10^{-2}\psi_0$ (1%) are obtained. This means that using the numerical approach is sufficiently good to simulate the system.

Once the concentration has been calculated, the flux at the interface and consequently the charge $Q(t)$ that enters the channel (see Eq. (2.32)) can be estimated. As shown in Figure 4.2, three regions are identified in the temporal evolution of $Q(t)$. In region I, defined for

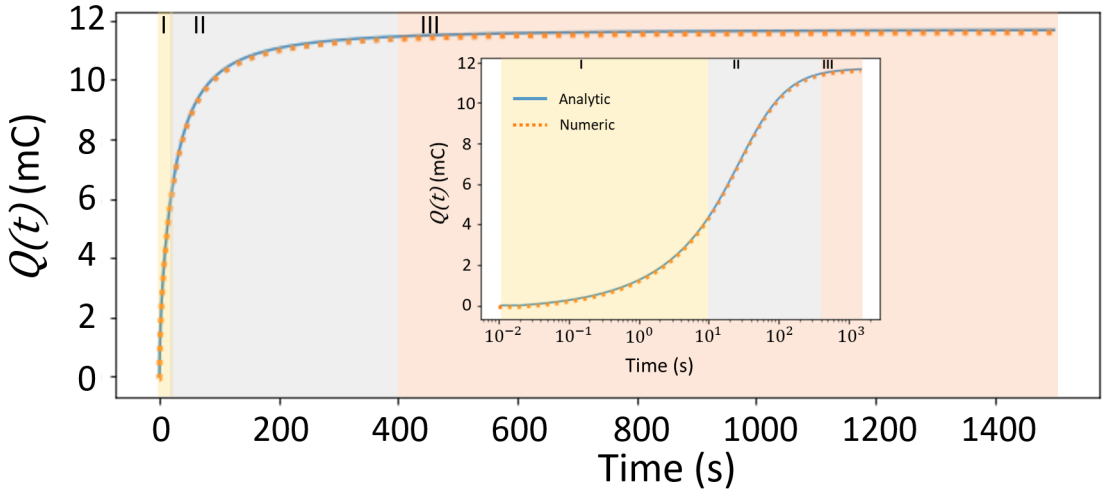

Figure 4.2 - Comparison between the numerical (dotted line) and analytical (solid line) results for charge $Q(t)$ entering in the channel.

Source: By the author.

$0.01 < t < 10\,\mathrm{s}$, a steep rise of $Q(t)$ is observed. Then, for $10 < t < 400\,\mathrm{s}$, $Q(t)$ increases at a slower rate in relation to the previous region. Further, the region II is characterized by an inflection point that flattens the curve. For times in the interval $400 < t < 1500\,\mathrm{s}$, the system achieves a quasi-constant value of $Q(t)$. At the beginning of OECT operation (region I), the cations placed close to the electrolyte-semiconductor interface will move rapidly towards the semiconductor due to the large concentration gradient near the interface (see Figure 4.1(a)). As the concentration profile broadens due to diffusion, the quantity of ions reaching the semiconductor decreases, which is reflected in the slower growth of $Q(t)$. At the moment at which the maximum concentration profile crosses the interface, an inflection point in $Q(t)$ is observed. At this point, most of the particle concentration is already in the channel. As a result, the flux reduces and consequently $Q(t)$ starts to converge. In the final interval, the flux vanishes, meaning that a new steady state is achieved. From Figure 4.2 it is also visible the good agreement between both numerical and analytical solutions.

As described in Section 2.2.2, the determination of $Q(t)$ allows one to study the drain current I_D by using of Bernard-Malliaras model. Aiming to a better interpretation of the results, each of the two following terms composing the I_D (see Equation (2.24)) are examined. The first term $I_1(t) = G\left(1 - \frac{Q(t)}{e\rho_0\nu}\right)V_D$ accounts to the charge $Q(t)$ that de-dopes the semiconductor, whereas the second term $I_2(t) = -f\frac{\mathrm{d}Q(t)}{\mathrm{d}t}$ is defined by the temporal derivative of the charge entering the material.

In Fig. 4.3, the temporal evolution of the change in I_D is displayed, which is divided into the same three regions defined for $Q(t)$ (see Figure 4.2). In the first one, the values obtained for I_D show a rapid decreasing behavior dominated by I_2, which arises from the strong growth of $Q(t)$ in the first $10\,\mathrm{s}$. For the next $200\,\mathrm{s}$, the variations in $Q(t)$ occurs at a very slow rate, which leads to the convergence of I_2 to zero. Therefore, from this time, the evolution of the drain current is principally dominated by I_1, which causes a similar behavior to the obtained for

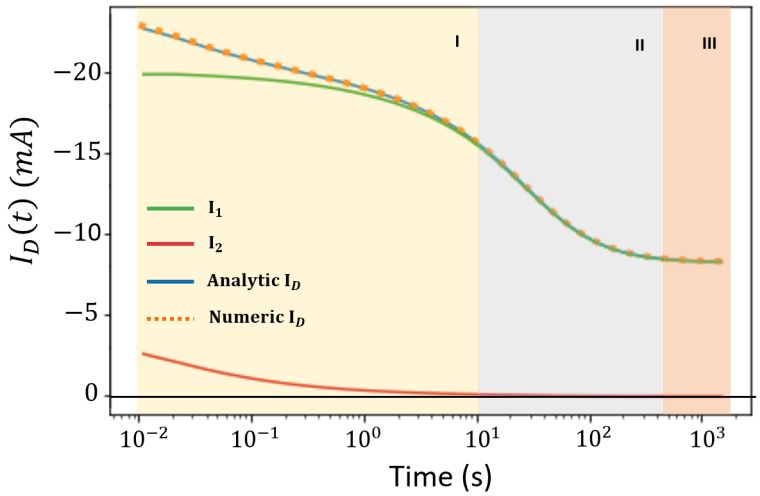

Figure 4.3 - Drain current obtained and the contribution of each term in the Bernards-Malliaras assumption.[44]
Source: By the author.

$Q(t)$ in regions II and III. As the system simulated represents a OECT that works on depletion mode (see Section 2.2), at the beginning the semiconductor channel is p-doped, which leads to the initial current observed in Fig. 4.3. When the cations enter the channel, the doping state of the material is reduced, which leads to a decrease in the drain current. In the situation simulated here, due to the open boundary condition, the steady state current is achieved once all the cations migrate from the electrolyte to the semiconductor. When flux coming from the electrolyte vanishes, changes in the doping level of the channel are no longer produced, leading to the constant current observed. Again, the result presented in Fig. 4.3 allow to confirm the good agreement between numerical and analytical results.

4.2 Boundary Conditions

In Section 3.3, it was discussed that analytical solutions only holds for open boundary on the right-hand side and zero-concentration at the left-hand side (see Eq. (2.30)). As shown in Section 4.1, this condition results in a vanishing concentration for long times rather than a steady state profile. Since this hardly represents a realistic situation, the numerical approach is now applied to closed boundaries using the conditions expressed in Eq. (3.4). As this implies variations in both sides of the region considered, different consequences may arise due to the modification of both boundary conditions. To analyze the impacts of each modification individually, two cases are analyzed. In the case I, the zero flux condition at $x = 2\,\mathrm{cm}$ is considered, but the condition $\psi(x = 0, t) = 0$ for $t > 0$ is maintained. On the other hand, in case II, the boundary conditions of the analytical model are substituted for the zero flux conditions. Therefore, in this case, the system is considered to have closed boundaries, which means that the concentration is confined. For the following calculations, a gate voltage $V_G = 5\,\mathrm{mV}$, a constant concentration in the electrolyte with amplitude ψ_0 and the same diffusion coefficient D in all regions are considered.

4.2.1 Case I

The temporal evolution of the concentration obtained for case I is presented in Figure 4.4(a). Since the concentration cannot cross the boundary to the right, an accumulation is observed in the semiconductor region. For larger times, however, a vanishing concentration within the device region is still observed.

The comparison of the drain currents obtained with the solution of the Coppedé's model[53] and of the case I is presented in Figure 4.4(b). Initially, as the concentration takes some time to achieve the boundary of the system, the two solutions are identical. Therefore, in the range $0.01 < t < 0.03\,\mathrm{s}$, the closed boundary condition in the right-hand side has no impact on the drain current. In the region II defined for $0.03 < t < 100\,\mathrm{s}$, the implementation of the right boundary produces bigger values of I_D in relation to Coppedé's solution. Here, as a consequence of the accumulation on the semiconductor region, the concentration gradients are smaller than in the open boundary case, which means that less charge is entering (and de-doping) the channel. Surprisingly, for $100 < t < 1500\,\mathrm{s}$, a raise in the drain current is observed.

The decrease of the concentration as well as the raise in the drain current for region III presented in Fig. 4.4, result from the boundary conditions considered. As introduced in Section 2.1, the Nernst-Planck equation defines the flux as a function of on the concentration and its gradient. The condition $\psi(x = 0, t) = 0$, however, does not ensure a zero value for the derivative at this point. As a result, a negative flux on the left side is created, *i.e.*, ions may leave the device region to the left side, resulting in the decreasing behavior of the concentration. Further, the negative flux produce a reduction of the concentration in the whole region, leading to an increase in the doping level of the semiconductor, and consequently, the growth of the drain current observed in the results. This reinforces, that the conditions used in the Coppedé's model are not proper to describe the system.

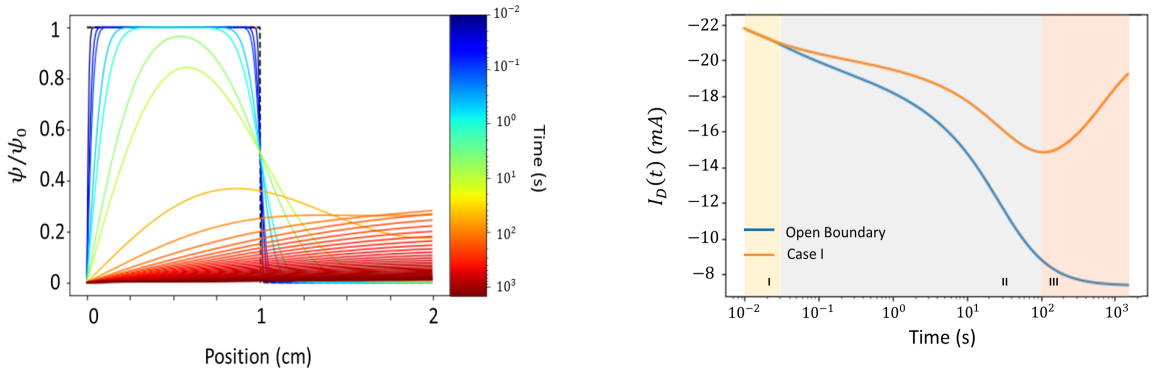

(a) (b)

Figure 4.4 - (a) Temporal evolution of concentration in case I. (b) Comparison of I_D between the results obtained for open boundaries and in case I.

Source: By the author.

4.2.2 Case II

Now, the case II previously mentioned is studied. Here, the zero-flux condition is implemented for both sides of the system (see Section (3.4)). In Figure 4.5, the temporal evolution of the concentration profiles for a system with closed boundaries is displayed. In this case, when the device is simulated for a time $t = 1500\,\mathrm{s}$, a convergence into a steady state is observed. In addition, a qualitative comparison with the analytical steady state solution (see Appendix D) allow to observe a good agreement between the numerical model and the theory. In difference to the results obtained when the conditions used in Coppedé's work[53] are implemented (see Figure 4.1(a)), the closed boundary condition ensure that the concentration remains in the desired region. Therefore, the implementation of closed boundaries allows simulating the evolution of the system from a transient behavior to a steady state.

Aiming to have a quantitative measurement of the quality in the results, the temporal evolution of the quantity $\Delta\psi = \frac{|\psi^{\mathrm{t}} - \psi^{\mathrm{n}}|}{N_x}$ is calculated. Here, ψ^{t} and ψ^{n} are the theoretical and numerical results, respectively. In Figure 4.6 the temporal evolution of $\Delta\psi$ is presented. At the beginning of the simulation, as ψ^{t} and ψ^{n} are very different, large values of $\Delta\psi$ are observed. As the system converges to a steady state, however, the values of $\Delta\psi$ decreases. From Figure 4.6, a convergence of $\Delta\psi$ to a constant curve is observed, which achieves values of $\sim 10^{-6}\psi_0$ for all grid points. Furthermore, the analysis of the temporal evolution of $\Delta\psi$ allow establishing that the steady state concentration is reached for times $t \geq 1200\,\mathrm{s}$, at which $\Delta\psi$ remains in a constant

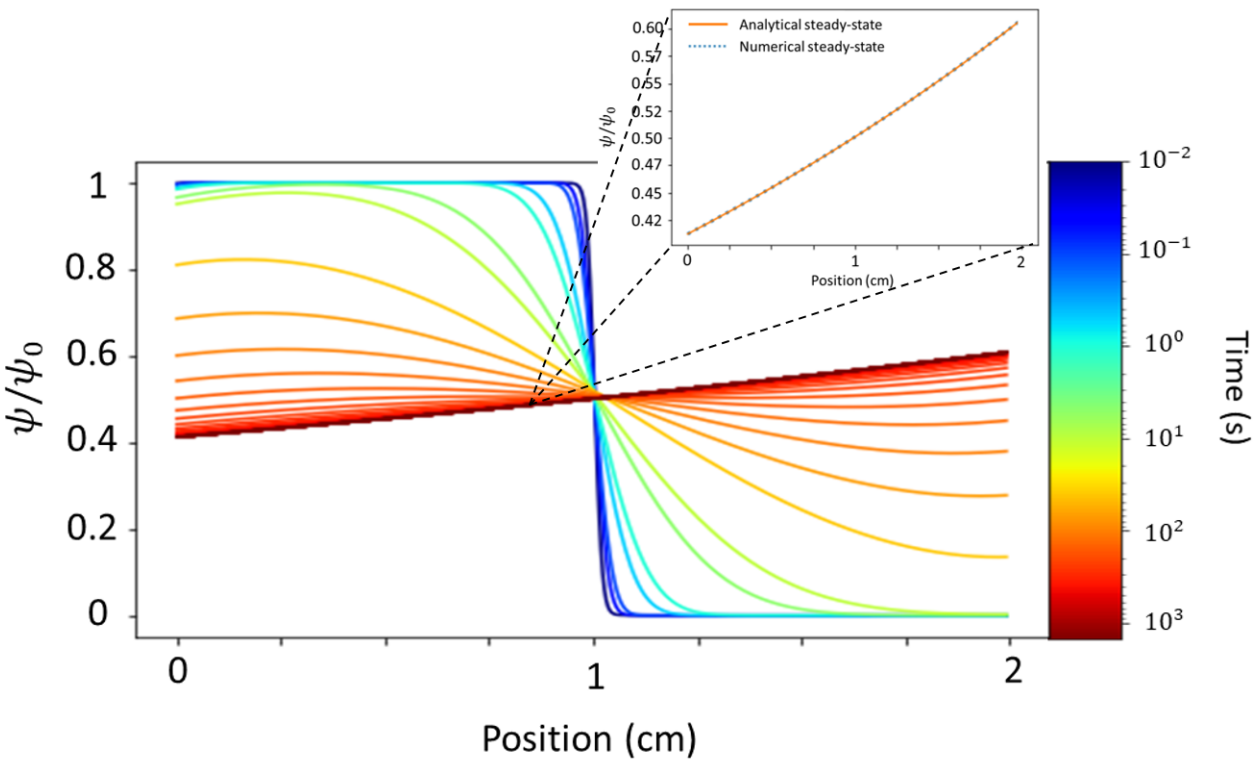

Figure 4.5 - Temporal evolution of concentration considering closed boundaries.
Source: By the author.

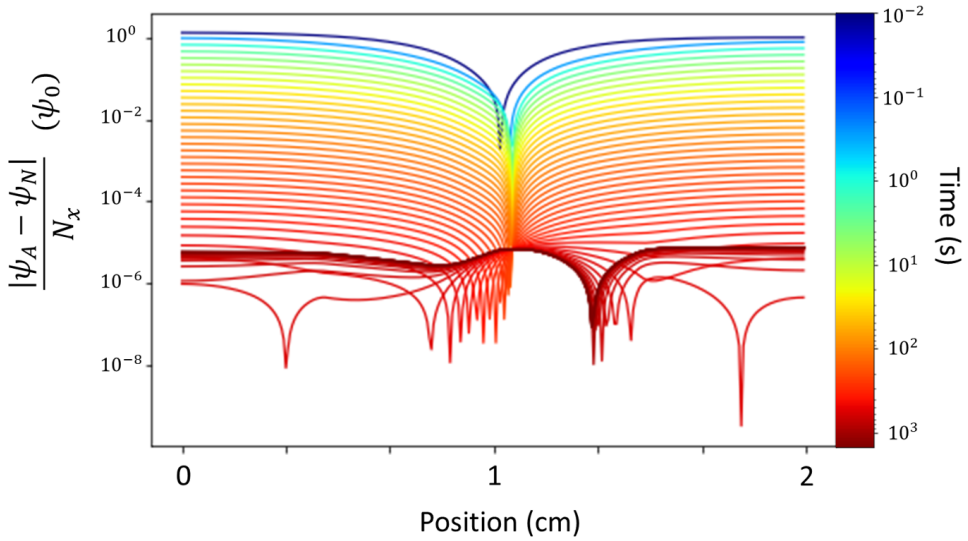

Figure 4.6 - Temporal evolution of $\Delta\psi$.
Source: By the author.

shape. Then, from this time, the migration of cations towards the channel can be considered as zero. The non-uniform distribution of $\Delta\psi$ is related to the errors introduced by the numerical artifacts inherent to the methods used. Note that, as a consequence of the non-uniform grid, at the electrolyte-semiconductor interface ($x = 1\,\mathrm{cm}$), where the separation between the points reaches the minimal value (see Section 2.3.6), $\Delta\psi$ decrease in magnitude. Overall, the results obtained for $\Delta\psi$ are reasonable values that permit to confirm the high accuracy in the numerical approximation.

Once the concentration is obtained, the flux at the interface is investigated. Figure 4.7(a) allow to develop an analysis of the impact that the boundary conditions have in the flux. Due to the logarithmic scale used in Figure 4.7(a), it is possible to identify that approximately for $t > 500\,\mathrm{s}$, the flux for open boundaries achieves an exponential profile. For the closed boundaries, however, the exponential behavior occurs after the first $100\,\mathrm{s}$. The result makes evident that when closed boundaries are considered, the flux tends to zero faster than if open boundaries are implemented. Further, it is established, as well, that the value for the flux at the steady state, defined previously to occur at $t = 1200\,\mathrm{s}$, achieves values of the order $\sim 10^{-12}\,\mathrm{mol/cm^2 s}$. Since in the open boundary case, the concentration has to spread over an infinitely long system, the convergence to a steady distribution of concentration occurs in a very slow rate. On the contrary, in the closed boundary case, the region allowed for the concentration to distribute is well-defined, which, as observed in Figure 4.7(a), allows for the system to achieve the steady state more quickly. Therefore, in relation to the flux, it is observed that boundary conditions have considerable impact in the time that the system needs to achieve a steady state, in which the flux vanishes.

As previously mentioned, the calculation of the flux allows to obtain the charge entering the semiconductor and consequently the drain current that flows between source and drain electrodes. Therefore, in order to establish the impact of the boundary conditions in the drain cur-

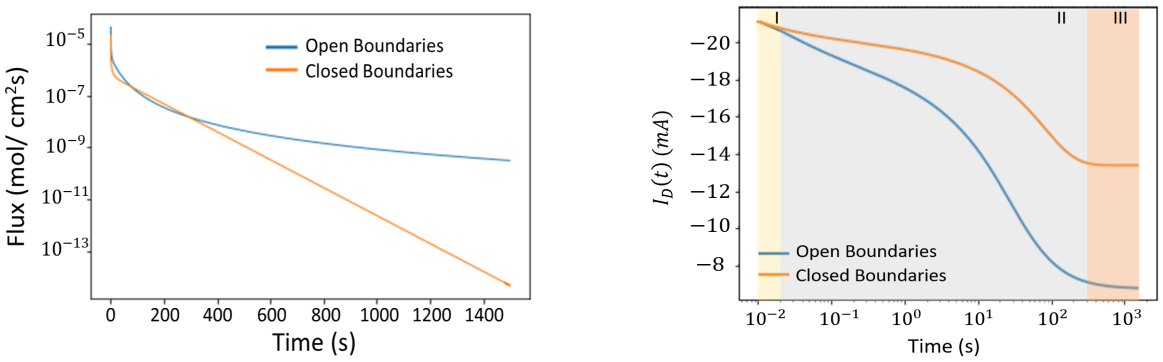

(a) (b)

Figure 4.7 - (a) Flux at the interface and (b) drain current for open and closed boundary cases.
Source: By the author.

rent, a comparison between the currents I_D^{CB} and I_D^{OB} obtained for closed and open boundaries, respectively, is developed.

From Figure 4.7(b), the same values for I_D^{CB} and I_D^{OB} can be observed in the interval $0.01 < t < 0.02\,\mathrm{s}$, which is related to the time that the concentration takes to feel the effect of the closed boundaries. Here, in difference to the case I (see Figure 4.4(b)), the system takes less time to be affected by the boundary conditions. For the rest of the time simulate ($0.02 < t < 1500\,\mathrm{s}$), values of $|I_D^{CB}| > |I_D^{OB}|$ are obtained. In the final interval, however, Figure 4.7(b) makes visible that in difference to I_D^{OB}, the value of I_D^{CB} is almost constant for times $t > 300\,\mathrm{s}$. The result $|I_D^{CB}| > |I_D^{OB}|$ observed in regions II and III is related to the quantity of ions that enters the channel. When closed boundaries are considered, the convergence of the system to a steady state distribution causes some part of the concentration to remain in the electrolyte. In the open boundary case, however, the concentration migrates from the electrolyte to the channel without any restriction, leading to larger reduction in the doping state of the material, and therefore, in I_D^{OB}. As discussed in the analysis of the flux, the system tends to achieve the steady state faster in the closed boundary case, which was established to occur at $t = 1200\,\mathrm{s}$. Hence, if closed boundaries are implemented, the doping level of the channel does not change anymore for $t > 1200\,\mathrm{s}$, which leads to the constant current observed in the results. On the contrary, in the open boundary case, the concentration continues migrating into the semiconductor, causing variations in I_D^{OB} for longer times.

It is important to mention that the time at which the steady current is achieved with closed boundaries is orders of magnitude larger than the obtained experimentally. This is caused by the value of the semiconductor and electrolyte thickness considered in the simulations, which in order to develop a comparison with the results obtained in the work of Coppedé is considered $T_e = T_{sc} = 1\,\mathrm{cm}$. As observed from the results, the boundary conditions have significant effects in the drain current, especially related to its values and the time that it takes to go from the initial state to the final steady state. At this point can be highlighted the importance to consider the correct boundary conditions in order to obtain results consistent with the expected

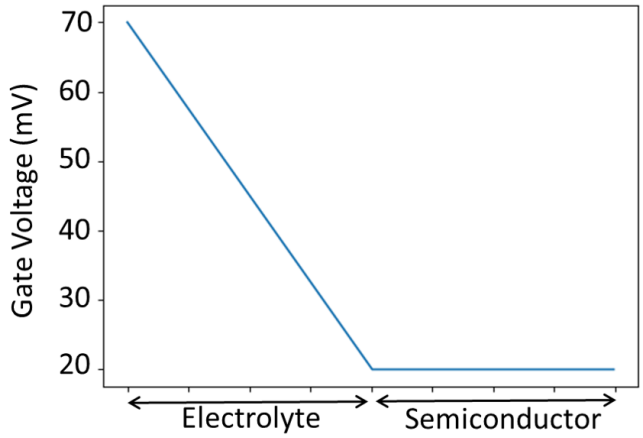

Figure 4.8 - Electric potential considered in the simulation.
Source: By the author.

experimentally. From this part, in all the results presented in the following sections, closed boundaries are considered.

4.3 Non-uniform electric field

As mentioned in Section 3.4, due to mixed conductive properties of organic semiconductors, a constant electric potential is generated inside the channel. Thus, in this section is considered the electric potential presented in Figure 4.8. Here, the values $V_G = 70\,\mathrm{mV}$, $T_{sc} = 1\,\mathrm{cm}$ and a constant cation concentration in the electrolyte of amplitude ψ_0 are considered. Additional relevant parameters are deposited in Table 3.1.

Once the electric field in one dimension is given by the derivative of the electric potential, *i.e.*, $E = \frac{\partial V}{\partial x}$, an electric field acting only in the region of the electrolyte is generated when this condition is implemented. In this situation, a marked difference in the temporal evolution of the concentration profiles for each region is observed (see Figure 4.9). In the electrolyte region, the concentration tends to converge to an exponential profile, which, according to the theory, it is the steady state solution for the Nernst-Planck equation (see Appendix D). As the electric field

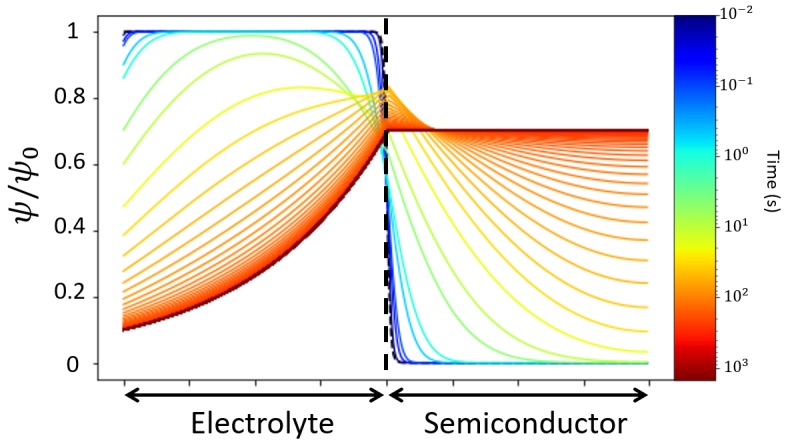

Figure 4.9 - Temporal evolution of the concentration considering a non-uniform electric field.
Source: By the author.

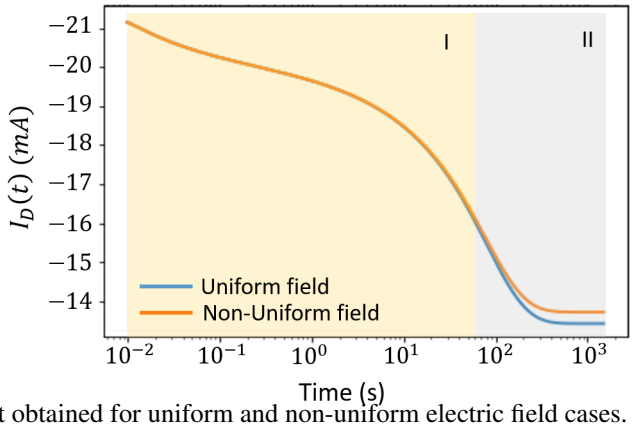

Figure 4.10 - Drain current obtained for uniform and non-uniform electric field cases.
Source: By the author.

in the semiconductor is zero, only diffusion processes are occurring within the material, which, as observed in Figure 4.9, results in a constant distribution of the concentration at the steady state.

Using the temporal evolution of the concentration, the charge entering the semiconductor, and consequently the drain current that flows between source and drain electrodes, can be determined. Therefore, in order to identify the impact of a non-uniform electric field, the drain current I_D is studied. As shown in Figure 4.10, for $t < 60\,\mathrm{s}$ (region I), the transient behavior of the current is similar to the obtained when a uniform field is considered. In the interval $60 < t < 1500\,\mathrm{s}$, however, as the system approaches the steady state, differences between the two results becomes more evident. Note that if a non-uniform electric field is implemented, the drain current I_D obtained at the steady state have bigger values than in the uniform electric field case. This means that with a non-uniform electric field, the semiconductor is less de-doped.

4.3.1 Variation in semiconductor thickness

In order to complement the study of the impact of this extension in the system, different values for the semiconductor thickness (T_{sc}) are considered. Here, T_{sc} varies from $0.03\,\mathrm{cm}$ to $1\,\mathrm{cm}$.

From the result shown in Figure 4.11(a), the consequences that the variation of T_{sc} have in the flux at the electrolyte-semiconductor interface, can be investigated. As displayed in Figure 4.11(a), the flux obtained with a uniform (solid line) and non-uniform (dotted line) electric field behave similarly for the different values of T_{sc}, showing differences only at large values of T_{sc}. For both cases, the reduction in T_{sc}, leads to a rapid convergence to steady state. This is produced because, with smaller values of T_{sc}, the region at which the cation concentration has to distribute is reduced, which makes the system able to reach the steady state faster.

Having the flux, the charge entering to the channel and consequently the drain current can be investigated using the Bernards-Malliaras model (see Section 2.2.2). Thus, an analysis of the drain current considering the variation in T_{sc} is developed. Figure 4.11(b) shows that for thin semiconductors, uniform and non-uniform fields produce the same stationary current. With large semiconductor thickness, however, bigger values of $\Delta I_D = I_D(t) - I_D(0)$, are obtained

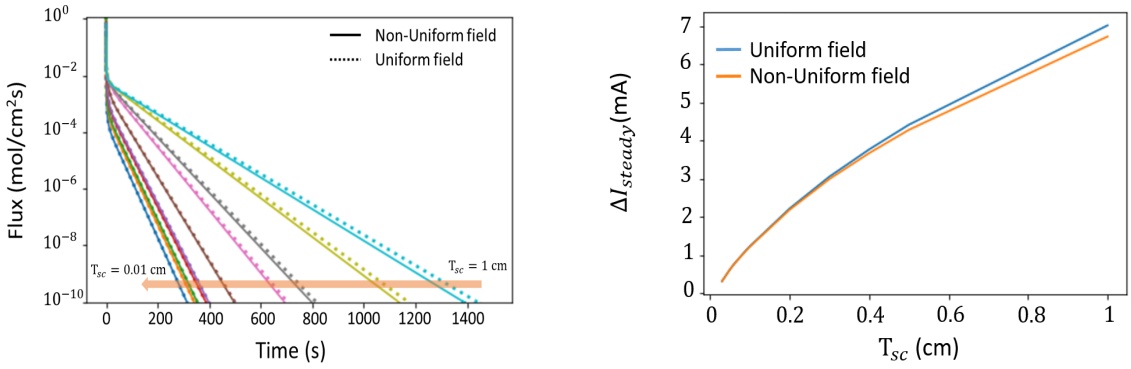

(a) (b)

Figure 4.11 - (a) Flux at the interface and (b) change of I_D at steady state as a function of the semiconductor thickness T_{sc}.

Source: By the author.

when a uniform field is considered (see Figure 4.11(b)). Therefore, the consideration of a non-uniform electric field impacts in the system mostly for channels with large thicknesses.

It is important to mention that electrolyte and semiconductor thicknesses considered in this work were chosen to obtain qualitative results with affordable computation times. As proven in Appendix B, if Δx decrease, smaller values of Δt must be considered, leading to an increase in the computational efforts needed to obtain a solution. Due to the limitation in the computational resources, devices with the dimensions obtained experimentally were not considered in this work. Therefore, the results discussed above provide a qualitative representation of the impact that different conditions have in the OECT functioning according to the drift-diffusion equations.

4.3.2 Variation of gate voltage

Now, a study of the drain current obtained at steady state (I_{steady}) as a function of the gate voltage V_G is developed. As presented in Figure 4.12, three different values for the semiconductor thickness are considered, which are $T_{sc} = 1\,\text{cm}$, $T_{sc} = 0.1\,\text{cm}$ and $T_{sc} = 0.03\,\text{cm}$. For the three cases, with uniform and non-uniform electric field, it is observed that as V_G grow, the current at the steady state turns smaller. The growth of V_G produces that the total quantity of ions that migrates into the semiconductor increases, which produces a decrease in the final doping level of the material, i.e., in I_{steady}. Considering a uniform electric field, however, it is observed that for the three semiconductor thicknesses, I_{steady} seems to be more affected by the variations of V_G. In the case where $T_{sc} = 1\,\text{cm}$, for $0 < V_G < 30\,\text{mV}$, a linear behavior is observed (see Figure 4.12(a)). For values $V_G > 30\,\text{mV}$, the decrease of the steady current slows down, which occurs due to the total quantity of ions that de-dopes the material. As V_G increases, the concentration remaining in the electrolyte at the steady state decreases. Consequently, the variations in the final doping level of the channel generated by the additional cations coming from the electrolyte, becomes smaller, leading to the slow reduction in I_{steady}. In the cases that $T_{sc} = 0.1\,\text{cm}$ and $T_{sc} = 0.03\,\text{cm}$, as the conductance of the material depends on the geometry of the channel

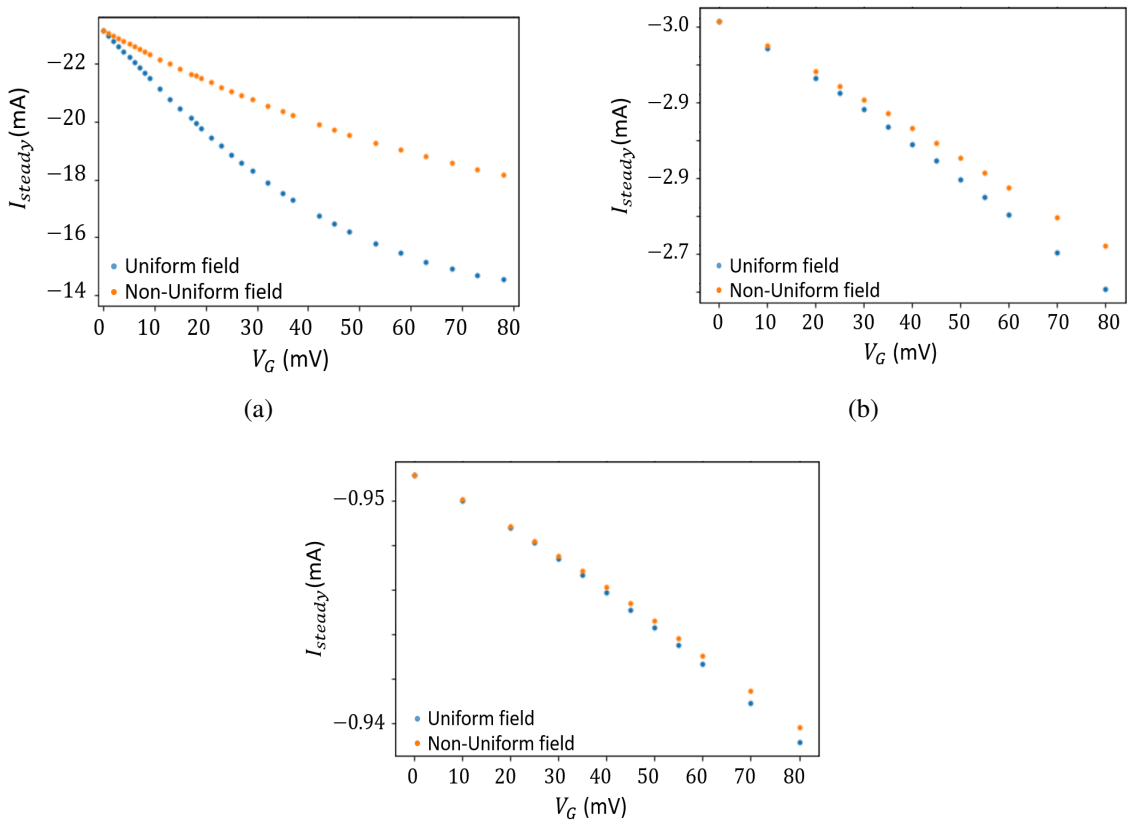

Figure 4.12 - Steady state current as a function of gate voltage for semiconductor thicknesses of (a) $1\,\mathrm{cm}$, (b) $0.1\,\mathrm{cm}$ and (c) $0.03\,\mathrm{cm}$.

Source: By the author.

(see Section 2.2.2), the currents obtained are smaller than with $T_{sc} = 1\,\mathrm{cm}$. Further, a linear behavior in relation to V_G is observed for these two values of T_{sc} (see Figure 4.12(b) and Figure 4.12(c)). If T_{sc} is reduced, the quantity of cations that enters the channel until the system achieves the steady state, decreases. For both cases ($T_{sc} = 0.1\,\mathrm{cm}$ and $T_{sc} = 0.03\,\mathrm{cm}$), most of the cations are in the electrolyte. Therefore, the linear reduction of I_{steady} will be observed until the voltage is high enough to produce that most of the cations to be in the channel.

4.4 Non-constant Diffusion Coefficient

As introduced in Section 3.5, the different morphologies and compositions of the materials produce variations in their characteristic parameters like the diffusion coefficient. Hence, different values for diffusion coefficients D_e and D_{sc} for the electrolyte and semiconductor region, respectively, are considered. For the following results, the information of the Table 3.1, a semiconductor of length $T_{sc} = 1\,\mathrm{cm}$ and the gate voltage represented in the Figure 4.8 are used. Furthermore, a constant initial concentration with the value ψ_0 in the electrolyte is implemented.

In Figure 4.13, the concentration profiles obtained for different combinations of D_e and D_{sc} are displayed. The results represent the system at a time $t = 1200\,\mathrm{s}$, which is the time needed for the reference case ($D_{sc} = D_e$) to achieve the steady state. In general, when a non-constant

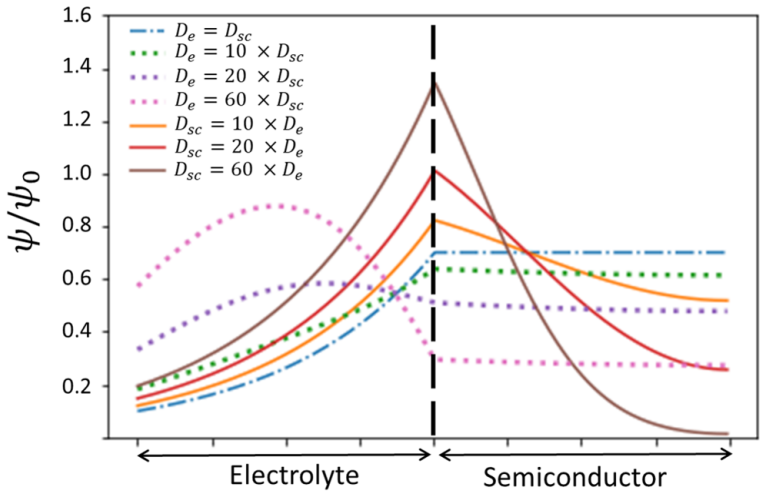

Figure 4.13 - Concentration profiles at $t = 1200\,\mathrm{s}$ for various combinations of diffusion coefficients.
Source: By the author.

diffusion coefficient is considered, the time required for the system to reach the steady state is affected. For all situations, the regions that present the smaller diffusion coefficient will take more time to achieve the profile expected. If $D_e < D_{sc}$, the formation of the exponential profile in the electrolyte due to the non-uniform electric field, is hindered. In the semiconductor, however, although a constant distribution is achieved, the value obtained is smaller than in the reference case, which reflects the difficulty of the ions to move within the electrolyte and migrate to the channel. In the other case, when $D_{sc} < D_e$, the exponential profile is created in the electrolyte, but the time is not enough for the system to achieve a constant concentration in the semiconductor. Here, the cations have more difficulty to distribute uniformly inside the organic semiconductor material.

As previously mentioned, the temporal evolution of the concentration allows to investigate the drain current that flows between source and drain electrodes. Thus, it is developed a qualitative study of the impacts in the drain current when different values of D_e and D_{sc} are considered. For this purpose, two cases are analyzed, which are: $D_{sc} < D_e$ and $D_{sc} > D_e$. For the former

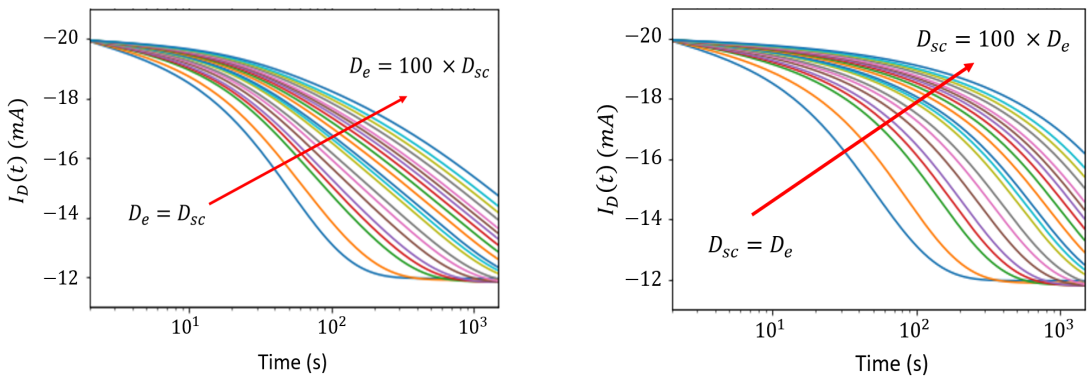

Figure 4.14 - Drain current for (a) fixed D_e but varying D_{sc} and (b) fixed D_{sc} but varying D_e.
Source: By the author.

case, a fixed diffusion coefficient $D_e = D$ (see Table 3.1) and a variable coefficient in the semiconductor given by $D_{sc} = \frac{D}{\omega}$, are used. Here, ω is a constant ranging from 1 to 100. For the latter case, which considers $D_{sc} > D_e$, the coefficients are defined as: $D_e = \frac{D}{\omega}$, $D_{sc} = D$. As observed in Figure 4.14, the reduction of both D_{sc} and D_e, leads to a shift of the drain current curve to larger times, *i.e.*, the time necessary to achieve the steady state current increases. However, the variation of D_e, leads to a larger shift of the curves, *i.e.*, the variation of D_e impacts the more in the evolution of the drain current from a transient behavior to the steady state. As the ions have more difficulty to migrate from the electrolyte to the semiconductor, the rate at which the de-doping processes occur decreases as D_e decrease. In the other case, if $D_{sc} < D_e$, the ions affected are already inside the semiconductor. Then, as the cations have facility to passing from the electrolyte to the semiconductor, the de-doping processes are less affected.

Here, the impact of the diffusion coefficient has been studied qualitatively in order to identify the variations that this assumption may cause in relevant quantities such as the drain current. Therefore, although the dimensions and parameters used for the device materials may differ from the ones obtained experimentally, the results provide insights of the possible effects in the OECT functioning when different scenarios are considered.

4.5 Chemical Potential

In order to highlight the different properties of the electrolyte and the organic semiconductor, the chemical potential as the driving force of diffusion is included into the numerical model. Here, the semiconductor thickness is $T_{sc} = 1\,\mathrm{cm}$ and the diffusion coefficient is equal in both regions.

First, the discussion of this consideration starts with the analysis of the case in which the difference in the standard chemical potential (see Section 3.5) is $\Delta\mu^0 = \mu^0_{sc} - \mu^0_e = -3\,\mathrm{kJ\,mol^{-1}}$, and no gate voltage is applied. In this case, the standard chemical potential in the organic semiconductor is smaller than in the electrolyte. Additionally, a constant initial concentration in all regions is considered. As displayed in Figure 4.15(a), in consequence to consider only diffusion processes, the steady state achieved is characterized by a constant concentration for each region. In the semiconductor region, however, a bigger value of the concentration is observed, which is a consequence of the chemical potential gradient generated by $\Delta\mu^0$ (see Equation (2.11)). Further, the introduction of the chemical potential generates a discontinuity in the concentration profile, which results from the so-called "uphill" diffusion[75] (see Figure 4.15(a)). Note that, although there exists a discontinuity in the concentration, at the steady state, the chemical potential takes a constant value, *i.e.*, the system achieves the equilibrium (see Figure 4.15(b)). Now, if $\Delta\mu^0 = 3\,\mathrm{kJ\,mol^{-1}}$, the concentration profiles show opposite behavior in relation to the previous case. Here, as shown in Figure 4.15(c) the "uphill" diffusion takes place in the direction of the electrolyte. Therefore, in the absence of an electric field, the value of $\Delta\mu^0$ establish the direction in which the ion migration occurs.

Once the implications of the introduction of the chemical potential were established, it is

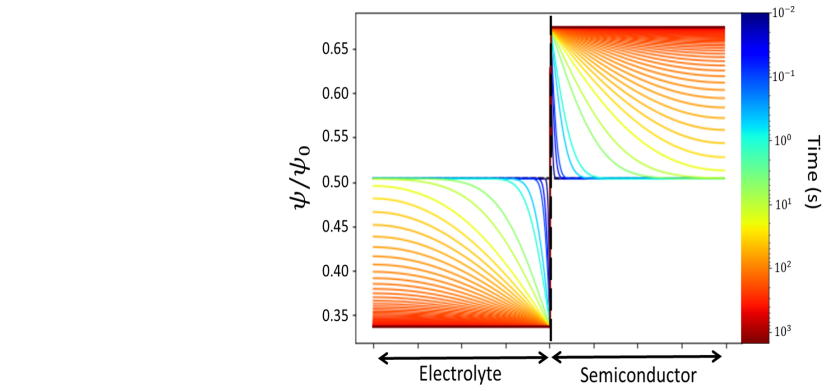

(a)

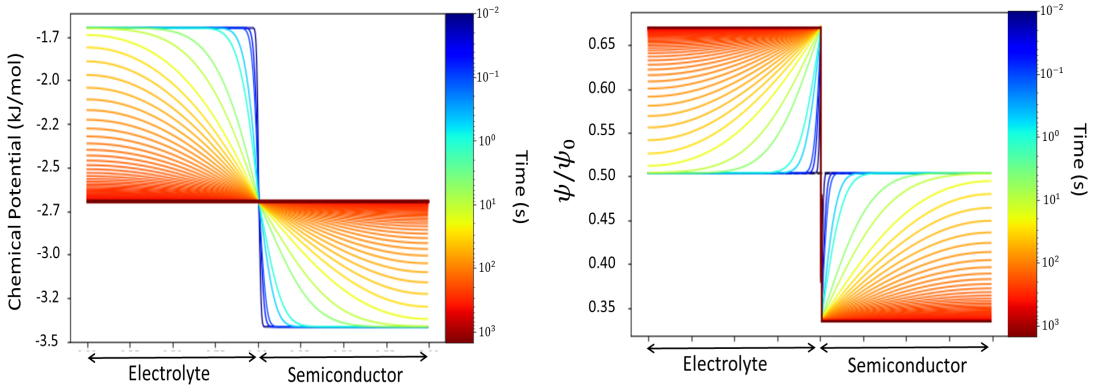

(b) (c)

Figure 4.15 - Temporal evolution of (a) the concentration and (b) chemical potential with $\Delta\mu^0 = -3\,\mathrm{kJ\,mol^{-1}}$. (c) Temporal evolution of the concentration $\Delta\mu^0 = 3\,\mathrm{kJ\,mol^{-1}}$.

Source: By the author.

studied the case in which the gate voltage presented in Figure 4.8, *i.e.*, a non-uniform electric field is applied on the system. As normally, the excess of concentration is in the electrolyte, for the following results, the concentration profile presented in Figure 4.16(a) is used as the initial condition. Further, a value $\Delta\mu^0 = -3\,\mathrm{kJ\,mol^{-1}}$ is considered. In this case, as shown in Figure 4.16(b), the discontinuity in the concentration observed previously is also obtained. As a consequence of the electric field, however, the concentration profiles show a different behavior for each region. In the electrolyte, the non-uniform electric field leads to the convergence of the concentration to an exponential profile at the steady state. On the other hand, as in the channel only diffusion process is occurring, the concentration converges to a constant value (see Figure 4.16(b)). Note that, because of the gate voltage applied, the chemical potential at the steady state is no longer uniform along the system (see Figure 4.16(c)). As introduced in Section 2.1, in this scenario, the flux J is defined by the gradient of the electrochemical potential. Hence, at steady state, *i.e.*, $J = 0$, the chemical potential must cancel the contribution associated with the electric potential at all points (see Figure 4.16(d)). From the above results, therefore, it is concluded that the situations simulated with the numerical model agree with the theory, which allows to confirm qualitatively the validity of the model.

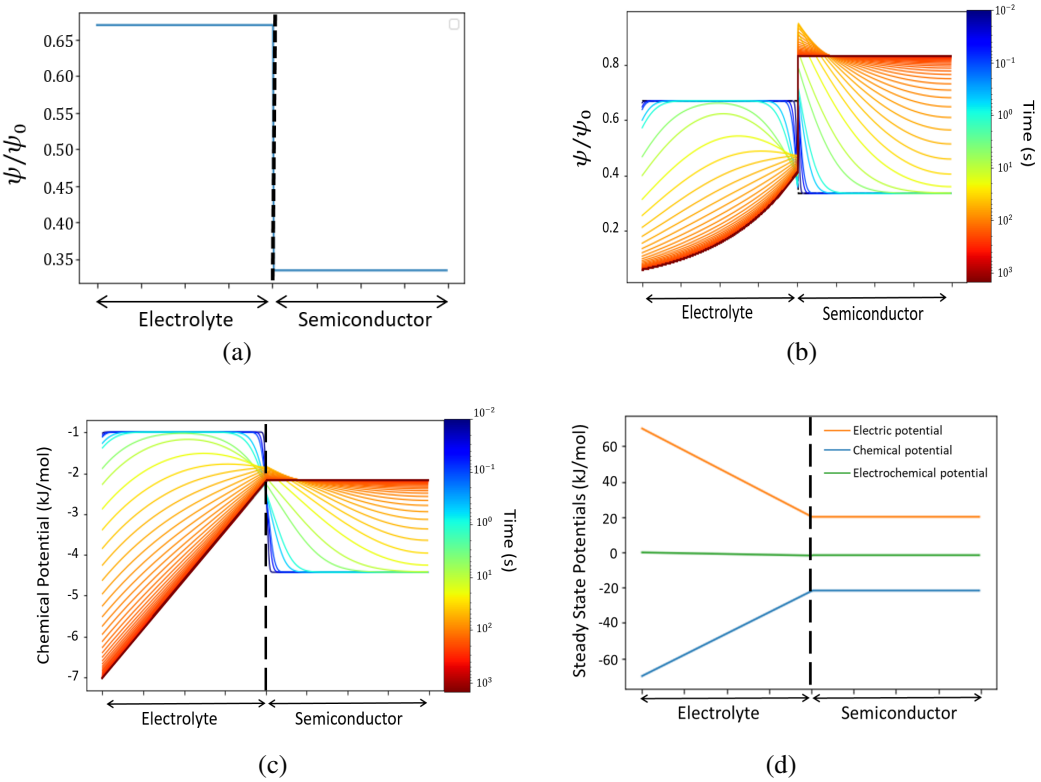

Figure 4.16 - (a) Initial concentration considered. (b) Temporal evolution of concentration and (c) chemical potential when a non-uniform electric field is applied. (d) Contribution of each term in the electrochemical potential at steady state.

Source: By the author.

Now, using the information obtained from the temporal evolution of the concentration, the time-dependent drain current I_D is analyzed. In Figure 4.17(b), the comparison of the system with $\Delta\mu^0 = -3\,\mathrm{kJ\,mol^{-1}}$ and $\Delta\mu^0 = 0$ is presented. Here, it is observed that in region I, the drain current obtained with $\Delta\mu^0 = -3\,\mathrm{kJ\,mol^{-1}}$ have larger values. During this interval, the current I_1 from the Bernards-Malliaras model (see Section 2.2.2) is equal in both cases (see Figure 4.17(a)). Nevertheless, for $\Delta\mu^0 = -3\,\mathrm{kJ\,mol^{-1}}$, I_2 shows bigger values, resulting in the differences observed initially for I_D. As the condition $\Delta\mu^0 = -3\,\mathrm{kJ\,mol^{-1}}$ enhances the cation migration towards the channel, larger variations of the charge $Q(t)$ that enters the material are produced, which leads to the significant contributions of I_2 observed in region I (see Figure 4.17(a)). From $3 < t < 1500\,\mathrm{s}$, the contribution of I_2 converges to zero, and I_1 defines the evolution of the system. As displayed in Figure 4.17(b), from this time, I_D turns smaller if $\Delta\mu^0 = -3\,\mathrm{kJ\,mol^{-1}}$. Since the chemical potential gradient created with $\Delta\mu^0 = -3\,\mathrm{kJ\,mol^{-1}}$, generates that more cations enter the semiconductor, the doping level of the material is reduced, and consequently a smaller drain current is obtained. Note that, although the stationary current achieved in the two cases is different, the time that the system needs to achieve the steady state is the same. Therefore, the variation of $\Delta\mu^0$ affects principally the quantity of ions that de-dopes the semiconductor, rather than the velocity at which the system converges to the steady state.

The temporal evolution of the I_D, however, may depend on the value of $\Delta\mu^0$ used. Thus, in

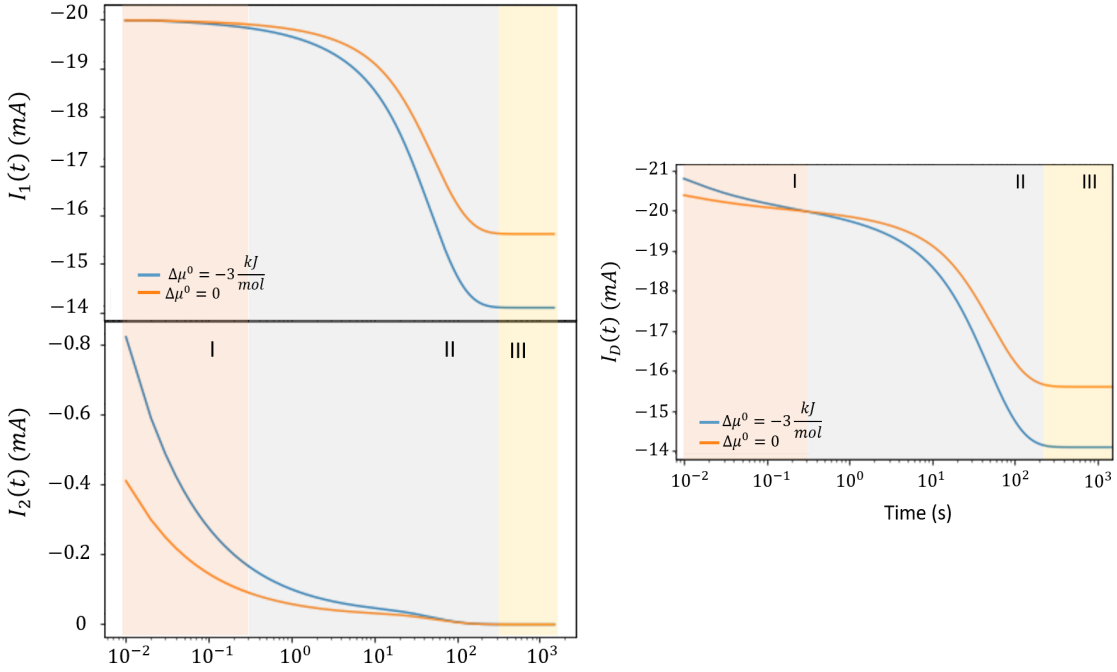

(a) (b)

Figure 4.17 - (a) Comparison of I_1 and I_2. (b) Drain current obtained considering the chemical potential.
Source: By the author.

order to investigate this dependence, various values of $\Delta\mu^0$ are considered. Here, $\Delta\mu^0$ will take values from $-3\,\mathrm{kJ\,mol^{-1}}$ up to $1.8\,\mathrm{kJ\,mol^{-1}}$. Previously, it was discussed that in the absence of an electric field, the value of $\Delta\mu^0$ defines the direction of the ion migration within the system. Therefore, if no gate voltage is applied, the system will achieve one different steady state concentration for each value of $\Delta\mu^0$ (see Figure 4.18(a)). In the case that $\Delta\mu^0 = 0$, the concentration tends to achieve a uniform distribution through the system. Thus, in order to study properly the dependence of the drain current on $\Delta\mu^0$, the initial concentration considered for each $\Delta\mu^0$ is their respective steady state concentration with $V_G = 0$, *i.e.*, $E = 0$.

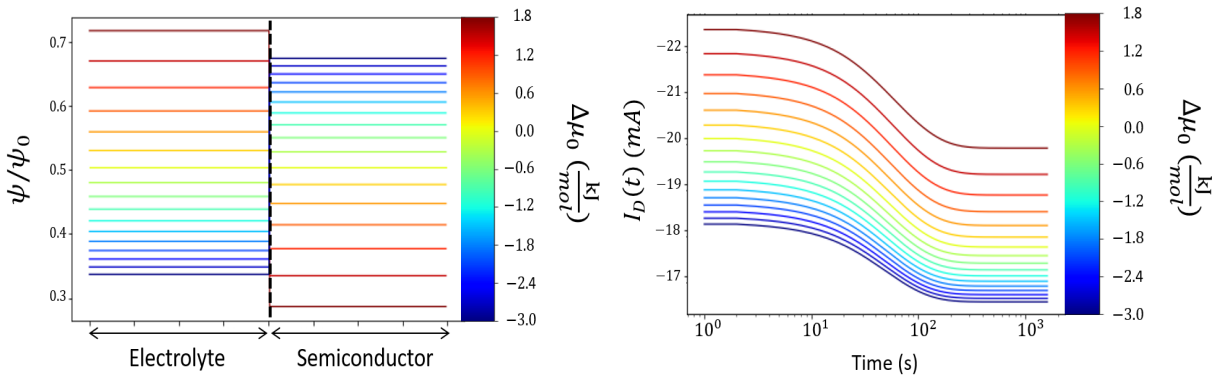

(a) (b)

Figure 4.18 - (a) Steady state concentration achieved for each value of $\Delta\mu^0$. (b) Drain current obtained with different values of $\Delta\mu^0$.
Source: By the author.

The different drain currents observed in Figure 4.18(b) at the beginning of the simulation, result from the initial doping state of the semiconductor. As mentioned earlier, for each value of $\Delta\mu^0$, one different concentration is considered as the initial condition. Thus, in each situation, the concentration considered defines the initial doping level of the channel. As in the cases where $\Delta\mu^0 < 0$, most of the cations are initially located at the semiconductor (see Figure 4.18(a)), the doping level (i.e. conductivity) of the material is low, which results in the small values of the initial current observed. When $\Delta\mu^0 > 0$, most of the cations are in the electrolyte, leading to a high doping level in the channel, and consequently large initial drain currents. In difference to the case when $\Delta\mu^0 < 0$, if $\Delta\mu^0 > 0$ more cations are allowed to enter the semiconductor in order to achieve the steady state. Therefore, the changes in the conductivity, *i.e.*, the drain current, are larger with $\Delta\mu^0 > 0$. Similarly with the result presented in Figure 4.16(c), although the variations of $\Delta\mu^0$ impacts the stationary current, the time that the system takes to achieve the steady state is not affected. Which confirms that, $\Delta\mu^0$ has consequences in the quantity of cations allowed to enter the semiconductor rather than in the time needed to achieve the equilibrium state. It is important to mention that the values considered here for $\Delta\mu^0$, were assumed aiming to obtain qualitative results that allow to investigate the impact of this parameter in the results. However, it is possible to calculate experimentally $\Delta\mu^0$ using different techniques.[97]

4.6 Time dependent gate voltage

Usually, to characterize the transient behavior of OECTs, temporal measurements of charge and discharge of the channel are developed applying a pulsed gate voltage. In this section, therefore, the evolution of the drain current applying a time dependent gate voltage is studied. The initial concentration showed in Figure 4.16(a), constant diffusion coefficient in all regions, $T_{sc} = 1\,\mathrm{cm}$, a non-uniform electric field and the value $\Delta\mu^0 = -3\,\mathrm{kJ\,mol^{-1}}$ are considered for the following calculations.

Initially, the square pulse displayed in Figure 4.19(a) is applied to the system. Note from

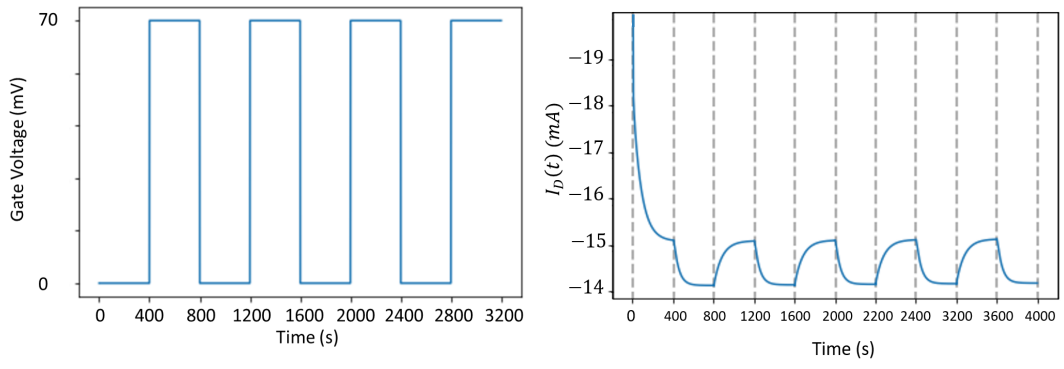

(a) (b)

Figure 4.19 - (a) Square pulse applied. (b) Drain current due to pulsed gate voltage.
Source: By the author.

Figure 4.19(b), that in the first $400\,\mathrm{s}$, as the gate voltage is zero, a slow reduction of the drain current is observed, which results from the diffusion of ions coming from the electrolyte. Then, for the next $400\,\mathrm{s}$ that the $V_G \neq 0$, as the cations in the electrolyte are forced to enter the semiconductor, the conductivity of the material, and consequently, the drain current decrease even more until achieve a new steady state. At the time that V_G is zero again, the system tend to converge to the previous steady state, and therefore, the excess of ion concentration diffuse in the direction of the electrolyte, leading to the increase in the conductivity of the material observed for times $800 < t < 1200\,\mathrm{s}$. From then, a periodic current is observed. These results show a good qualitative agreement to the experimental measurements reported in literature.[56,98]

An advantage of the numerical approach is that it allows to use any form of gate voltage. Here, square, triangular (Figure 4.20(a)) and saw-tooth (Figure 4.20(b)) type pulses are used to develop a study about the impact of each one in the drain current. If a triangular pulse is applied, a softer oscillatory curve is obtained. In this case, however, it is observed that the minimum drain current achieved is bigger in relation to the square pulse (see Figure 4.20(c)). When a saw-tooth pulse is applied, the drain current curve becomes sharpest, but similarly to the triangular pulse, the minimum current obtained is bigger than the obtained with the square pulse. Differently to the square pulse, in the triangular and saw-tooth pulses, the slow growth in the gate voltage causes that the movement of ions towards the channel to occur slowly as well.

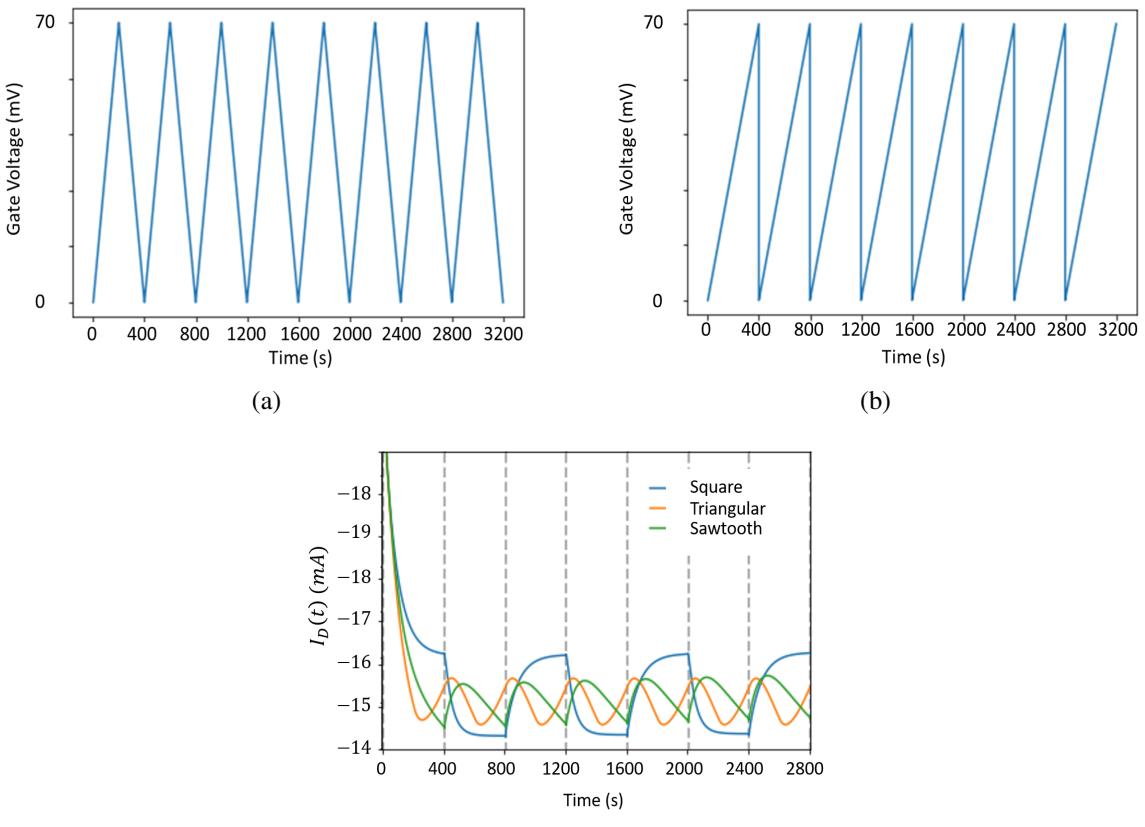

Figure 4.20 - (a) Triangular Pulse. (b) Sawtooth type pulse. (c) Drain current for each drain voltage.
Source: By the author.

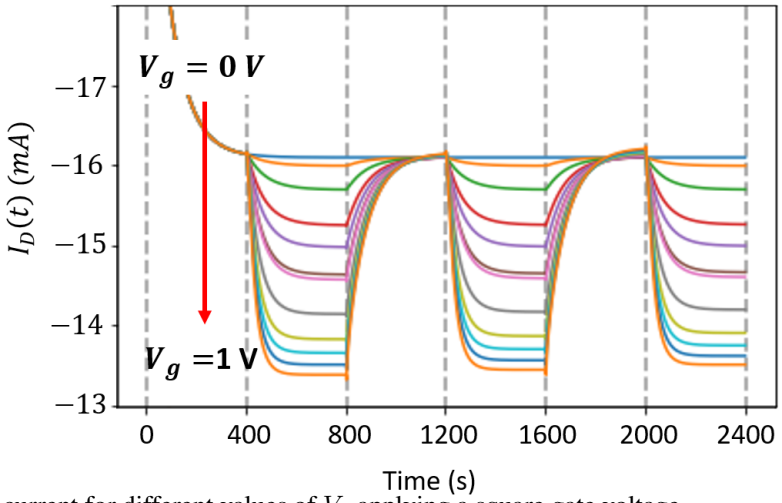

Figure 4.21 - Drain current for different values of V_g applying a square gate voltage.
Source: By the author.

Therefore, for these two pulses, the time is not enough for the system to achieve the new steady state. Further, as in the square and saw-tooth pulse the potential is turned off periodically for every $400\,\mathrm{s}$, the behavior of the current for the two pulses at this time is very similar.

Now, square-type pulses with different amplitudes are used to investigate the behavior of the drain current obtained. From Figure 4.21, it is observed that the drain current at the steady state tends to decrease as the gate voltage increase. Here, each value of V_G leads the system to reach a different steady state, *i.e.*, a different steady state drain current. The increase of V_G cause that the total quantity of cations entering and de-doping the channel increase as well, resulting in smaller values of the steady state drain currents.

In the following, various values of $\Delta\mu^0$ are considered to investigate its impact in the response of the system to a pulsed gate voltage. Here, a square-type gate voltage and the values of $\Delta\mu^0$ in the range of $-3\,\mathrm{kJ\,mol^{-1}}$ up to $1.8\,\mathrm{kJ\,mol^{-1}}$ are used. As mentioned in the previous section, for each value of $\Delta\mu^0$, distinct steady state concentrations are obtained in the absence of a gate voltage. Therefore, for the following results, the initial conditions displayed in Figure 4.18(a) are used again. At the first $400\,\mathrm{s}$ that the pulse is in the OFF state, it is observed from Figure 4.22 that for all values of $\Delta\mu^0$, no changes in the drain current are generated. This is because the initial condition for each $\Delta\mu^0$ is the steady state concentration obtained with $V_G = 0$. Hence, as the system is already in equilibrium, no migration of cations is produced. Then, for the next $400\,\mathrm{s}$ that the gate voltage is activated, the reduction of the drain current due to the drift of ions is observed. In Figure 4.22 can be seen that as $\Delta\mu^0$ turns positive, the difference between the initial and the final steady state value of the drain current increases. As previously discussed, the initial concentration on every case defines the initial doping state of the channel. Therefore, given that for the case in which $\Delta\mu^0 > 0$, most of the concentration is initially in the electrolyte, the quantity of cations that can migrate to the material under the application of a gate voltage is bigger. For all cases, a periodic current is observed after the first $400\,\mathrm{s}$. It is important to mention that due to the thickness used for the semiconductor, the times considered

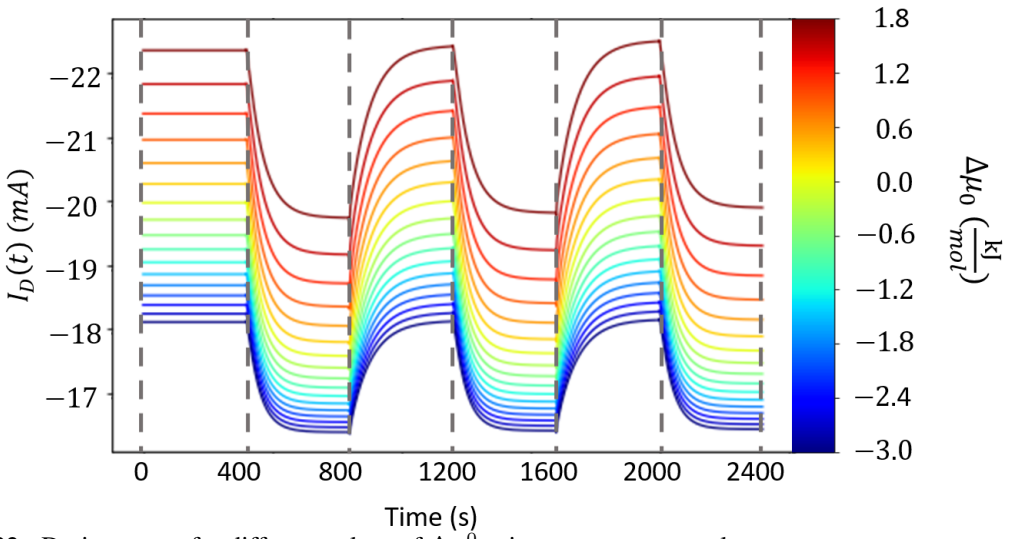

Figure 4.22 - Drain current for different values of $\Delta\mu^0$ using a square gate voltage.
Source: By the author.

for the pulses are orders of magnitude higher than those used experimentally. Therefore, these studies provide qualitative results that allow to identify the possible impact of each situation in the characterization of OECTs.

5 Conclusions

Organic electrochemical transistors (OECTs) have evolved as fundamental devices for emerging technologies. They have attracted widespread interest, accompanied by a steady improvement in its performance. In order to get a more profound understanding of the underlying mechanism, however, theoretical models capable to predict experimental data are still missing. In this project, a numerical approach is followed to solve the Nernst-Planck equation in one dimension, and model the ion migration from the electrolyte to the semiconductor. This allowed to elaborate an extensive study on the transient behavior of OECTs working in depletion mode.

In line with the objectives proposed in this project, to evaluate the accuracy of the implementation, standard boundary conditions used in the literature to solve analytically the drift-diffusion equations were considered. In doing so, the numerical results were in good agreement with the analytical solutions, achieving maximum errors of 1%. It was then discussed that these boundary conditions do not represent properly OECTs, since they consider a semiconductor layer with thickness tending to infinity, rather than a system with defined size. Aiming to simulate more accurately OECTs, boundary conditions which ensure a zero flux at finite boundaries were implemented. When this closed boundaries were considered, the temporal evolution of the concentration profiles showed a convergence to an exponential steady-state distribution, which is in good agreement with the result expected theoretically. Therefore, the introduction of the proper boundary conditions in the numerical implementation allowed to effectively describe the transient behavior from an initial state to a final steady state. The impact of each boundary condition in quantities like flux at the interface and the resulting drain current was investigated. In difference to the open boundary case, closed boundaries yield an exponentially decaying flux. This behavior is reflected in the drain current I_D, which achieves a steady state faster when closed boundaries are considered. Further, the value of I_D at the steady-state showed different values depending on the boundary conditions.

The mixed conductive property of the organic semiconductors, produces that the electronic charge carriers within the material react to any electric field applied to the semiconducting film. Following the Born–Oppenheimer approximation, the movement of electronic charge carriers is much faster than the diffusion motion of ions. Consequently, the electronic charges are quickly rearranged to compensate the electric field applied. Therefore, a non-uniform electric field, which is finite in the electrolyte region and zero in the semiconductor, was added to the model. However, the introduction of this condition produced an indeterminacy in the calculation of the numerical derivatives at the interface, which leads to a lost in the information of the concentration at that point. Aiming to solve this problem, the addition of this concentration by hand was proposed, which allowed to maintain the consistency in the results and ensure the conservation of particles within the system. With the application of a non-uniform electric field, different behaviors of the concentration were obtained in each region. On the one hand, an exponential

profile was achieved in the electrolyte at the steady state. On the other hand, as in the semiconductor only diffusion processes occur, a convergence to a constant concentration was observed. Although similar behaviors were identified in the drain current for uniform and non-uniform electric field, as the system approximate to the steady-state, a smaller value of I_D was obtained for the uniform electric field case. The analysis of various situations like different gate voltages (V_G), and different semiconductor thicknesses (T_{sc}) provided relevant information about the implication of this condition. The study of I_D at the steady state in function of the semiconductor thickness, showed that for small T_{sc}, the results obtained were the same for both uniform and non-uniform electric field. As the semiconductor thickness increases, however, a greater change in the drain current was obtained in the uniform electric field case. For different values of V_G, it was observed that as the gate voltage increases, more cations enter to the semiconductor channel, leading to a large decrease in the doping level of the material, and consequently the steady state drain current. For all gate voltages, the change in the drain current obtained for a uniform electric field was smaller than with a non-uniform electric field.

In order to consider the distinct compositions in electrolytes and semiconductors, different values of diffusion coefficients were introduced for each region. This extension has visible impacts in the time that the system needs to achieve the steady state. Furthermore, it was observed that the decrease in the diffusion coefficient of the electrolyte, have more impact in the evolution of the system from a transient to a steady behavior.

The introduction of the chemical potential as the driving force of diffusion leaded to significant variations in the results obtained with the model. Here, to reflect the distinction in the properties of each material, different standard chemical potentials for the electrolyte and the organic semiconductor region were considered. The implementation of this extension produced the so-called "uphill" diffusion reported in the literature. In this situation, the results obtained agreed with the theory, which allowed to confirm qualitatively the validity of the situations described with the numerical implementation. Further, the drain current showed to be affected when this consideration is introduced in the model.

Finally, a time dependent gate voltage was considered, which allowed to simulate a charge and discharge processes of OECTs. Besides, with the numerical method, it was possible to implement different types of pulsed potentials and investigate the impact of each one in the currents obtained. For all cases, oscillatory curves similar to experimental measurements were obtained.

As observed from previous discussion, the numerical approach allowed to investigate qualitatively several situations that goes beyond the analytical description. However, various limitations were found along the development of this work. The principal limitation was associated to computational resources required to obtain a solution in reasonable periods of time. For example, although different semiconductor lengths were investigated, the dimensions of the devices simulated are still orders of magnitude bigger than the obtained experimentally. According to the stability condition of the numerical scheme, the consideration of smaller semiconductor and

electrolyte thicknesses, *i.e.*, Δx, leads to the necessity to use smaller time steps Δt. By doing so, a considerable increase in the computational resources was generated in order to obtain results in affordable times.

The results obtained with the numerical model presented in this dissertation, allowed to obtain a description of the transient behavior of OECTs working in depletion mode. In the previous results, the values of parameters such as diffusion coefficients and standard chemical potentials, were assumed aiming to investigate qualitatively their impact on the results obtained when the OECTs are simulated. However, several techniques reported in the literature,[97,99] may be used to measure and calculate experimentally these parameters, and use them in the model. Thus, it is important to combine efforts with experimental works to improve the modeling of these devices. Aiming to overcome some limitations of this implementation, the algorithms used here could be optimized, which may allow the simulation of devices with the proper dimensions. Further, it may be interesting to include additional conditions into the model. For example, in all situations investigated in this work, only one ionic specie was considered in the calculations. Thus, aiming to model more accurate situations, interaction between the two types of ions and its impact in the results could be investigated. Besides, this model is based on one dimensional equation. Therefore, to consider effects such as lateral ionic currents,[51] to extend the model to higher dimensions is still necessary. This extension could represent a relevant improvement in the field of OECTs simulation.

References

1 BLYTHE, A. R. *et al.* **Electrical properties of polymers**. Cambridge: Cambridge university press, 2005.

2 INZELT, G. Rise and rise of conducting polymers. **Journal of Solid State Electrochemistry**, Springer, v. 15, n. 7, p. 1711–1718, 2011.

3 BOLTO, B. A.; WEISS, D.; WILLIS, D. Electronic conduction in polymers. V. aromatic semiconducting polymers. **Australian Journal of Chemistry**, CSIRO Publishing, v. 18, n. 4, p. 487–491, 1965.

4 BOLTO, B. A.; MCNEILL, R.; WEISS, D. Electronic conduction in polymers. III. electronic properties of polypyrrole. **Australian Journal of Chemistry**, CSIRO Publishing, v. 16, n. 6, p. 1090–1103, 1963.

5 ELSCHNER, A. *et al.* **PEDOT:** principles and applications of an intrinsically conductive polymer. Boca Raton: CRC press, 2010.

6 KUMAR, R.; SINGH, S.; YADAV, B. Conducting polymers: synthesis, properties and applications. **International Advanced Research Journal in Science, Engineering and Technology**, v. 2, n. 11, p. 110–124, 2015.

7 SHIRAKAWA, H. *et al.* Synthesis of electrically conducting organic polymers: halogen derivatives of polyacetylene,(CH)x. **Journal of the Chemical Society, Chemical Communications**, Royal Society of Chemistry, n. 16, p. 578–580, 1977.

8 CHIANG, C. *et al.* Electrical conductivity in doped polyacetylene. **Physical Review Letters**, APS, v. 40, n. 22, p. 1472, 1978.

9 NOBEL MEDIA. **Nobel Prize in Chemistry**. 2000. Available in:⟨https://www.nobelprize.org/prizes/chemistry/2000/summary/⟩, Accessed on 2022-03-05.

10 NAMSHEER, K.; ROUT, C. S. Conducting polymers: A comprehensive review on recent advances in synthesis, properties and applications. **RSC Advances**, Royal Society of Chemistry, v. 11, n. 10, p. 5659–5697, 2021.

11 KALONI, T. P. *et al.* Polythiophene: from fundamental perspectives to applications. **Chemistry of Materials**, ACS Publications, v. 29, n. 24, p. 10248–10283, 2017.

12 YEN, H.-J. *et al.* Development of conjugated polymers for memory device applications. **Polymers**, Multidisciplinary Digital Publishing Institute, v. 9, n. 1, p. 25, 2017.

13 LI, Y.; SHEN, Y. Polythiophene-based materials for nonvolatile polymeric memory devices. **Polymer Engineering & Science**, Wiley Online Library, v. 54, n. 11, p. 2470–2488, 2014.

14 PILLAI, R. G. *et al.* Field-induced carrier generation in conjugated polymer semiconductors for dynamic, asymmetric junctions. **Advanced Materials**, Wiley Online Library, v. 20, n. 1, p. 49–53, 2008.

15 LIANG, Y.; YU, L. A new class of semiconducting polymers for bulk heterojunction solar cells with exceptionally high performance. **Accounts of Chemical Research**, ACS Publications, v. 43, n. 9, p. 1227–1236, 2010.

16 GALPERIN, M.; NITZAN, A. Molecular optoelectronics: the interaction of molecular conduction junctions with light. **Physical Chemistry Chemical Physics**, Royal Society of Chemistry, v. 14, n. 26, p. 9421–9438, 2012.

17 TSUMURA, A.; KOEZUKA, H.; ANDO, T. Macromolecular electronic device: Field-effect transistor with a polythiophene thin film. **Applied Physics Letters**, American Institute of Physics, v. 49, n. 18, p. 1210–1212, 1986.

18 ADMASSIE, S. *et al.* A polymer photodiode using vapour-phase polymerized PEDOT as an anode. **Solar Energy Materials and Solar Cells**, Elsevier, v. 90, n. 2, p. 133–141, 2006.

19 ARIAS, A. *et al.* Organic photodiodes using polymeric anodes. **Synthetic Metals**, Elsevier, v. 102, n. 1-3, p. 953–954, 1999.

20 OUYANG, J. *et al.* Highly conductive PEDOT:PSS film and its applications in optoelectronic devices. **Advanced Functional Materials**, v. 15, p. 203–208, 2005.

21 WEI, Q. *et al.* Polymer thermoelectric modules screen-printed on paper. **RSC Advances**, Royal Society of Chemistry, v. 4, n. 54, p. 28802–28806, 2014.

22 ZHU, Z. *et al.* Significant conductivity enhancement of PEDOT:PSS films treated with lithium salt solutions. **Journal of Materials Science:** Materials in Electronics, Springer, v. 26, n. 1, p. 429–434, 2015.

23 SUN, K. *et al.* Review on application of PEDOTs and PEDOT:PSS in energy conversion and storage devices. **Journal of Materials Science:** Materials in Electronics, Springer, v. 26, n. 7, p. 4438–4462, 2015.

24 AMANCHUKWU, C. V. *et al.* Evaluation and stability of PEDOT polymer electrodes for LI–O2 batteries. **The Journal of Physical Chemistry Letters**, ACS Publications, v. 7, n. 19, p. 3770–3775, 2016.

25 SINHA, S. K. *et al.* Screen-printed PEDOT:PSS electrodes on commercial finished textiles for electrocardiography. **ACS Applied Materials & Interfaces**, ACS Publications, v. 9, n. 43, p. 37524–37528, 2017.

26 COLUCCI, R. *et al.* Cross-linked PEDOT:PSS as an alternative for low-cost solution-processed electronic devices. **Synthetic Metals**, Elsevier, v. 241, p. 47–53, 2018.

27 GHOSEKAR, I. C.; PATIL, G. C. Review on performance analysis of P3HT:PCBM-based bulk heterojunction organic solar cells. **Semiconductor Science and Technology**, IOP Publishing, v. 36, n. 4, p. 045005, 2021.

28 LUDWIGS, S. **P3HT revisited-from molecular scale to solar cell devices**. Berlin: Springer, 2014. v. 265.

29 GUEYE, M. N. *et al.* Progress in understanding structure and transport properties of PEDOT-based materials: A critical review. **Progress in Materials Science**, Elsevier, v. 108, p. 100616, 2020.

30 JIANG, L. *et al.* Blue spectral shift of P3HT organic film by KrF excimer laser ablation. *In*: INTERNATIONAL CONFERENCE ON OPTICAL INSTRUMENTS AND TECHNOLOGY: OPTOELECTRONIC DEVICES AND INTEGRATION, 2009, Shanghai. **Proceedings** [...]. Shanghai: Shanghai University of Science and Technology. 2009. p. 117–125.

31 SHAW, J. M.; SEIDLER, P. F. Organic electronics: introduction. **IBM Journal of Research and Development**, IBM, v. 45, n. 1, p. 3–9, 2001.

32 KELLEY, T. W. *et al.* Recent progress in organic electronics: Materials, devices, and processes. **Chemistry of Materials**, ACS Publications, v. 16, n. 23, p. 4413–4422, 2004.

33 SOUHARCE, B. *et al.* Amorphous carbazole-based (co) polymers for ofet application. **Macromolecular Rapid Communications**, Wiley Online Library, v. 30, n. 14, p. 1258–1262, 2009.

34 HE, Z. *et al.* Simultaneous enhancement of open-circuit voltage, short-circuit current density, and fill factor in polymer solar cells. **Advanced Materials**, Wiley Online Library, v. 23, n. 40, p. 4636–4643, 2011.

35 SUGIMOTO, A. *et al.* Flexible oled displays using plastic substrates. **IEEE Journal of Selected Topics in Quantum Electronics**, IEEE, v. 10, n. 1, p. 107–114, 2004.

36 RIVNAY, J. *et al.* Organic electrochemical transistors. **Nature Reviews Materials**, Nature Publishing Group, v. 3, n. 2, p. 1–14, 2018.

37 WHITE, H. S.; KITTLESEN, G. P.; WRIGHTON, M. S. Chemical derivatization of an array of three gold microelectrodes with polypyrrole: fabrication of a molecule-based transistor. **Journal of the American Chemical Society**, ACS Publications, v. 106, n. 18, p. 5375–5377, 1984.

38 NILSSON, D. *et al.* Electrochemical logic circuits. **Advanced Materials**, Wiley Online Library, v. 17, n. 3, p. 353–358, 2005.

39 GKOUPIDENIS, P. *et al.* Synaptic plasticity functions in an organic electrochemical transistor. **Applied Physics Letters**, AIP Publishing LLC, v. 107, n. 26, p. 263302, 2015.

40 MIKHNENKO, O. V.; COLLINS, S. D.; NGUYEN, T.-Q. Rectifying electrical noise with an ionic-organic ratchet. **Advanced Materials**, Wiley Online Library, v. 27, n. 12, p. 2007–2012, 2015.

41 SMELA, E. Conjugated polymer actuators for biomedical applications. **Advanced Materials**, Wiley Online Library, v. 15, n. 6, p. 481–494, 2003.

42 RIVNAY, J. *et al.* High-performance transistors for bioelectronics through tuning of channel thickness. **Science Advances**, American Association for the Advancement of Science, v. 1, n. 4, p. e1400251, 2015.

43 LIN, P. *et al.* The application of organic electrochemical transistors in cell-based biosensors. **Advanced Materials**, Wiley Online Library, v. 22, n. 33, p. 3655–3660, 2010.

44 BERNARDS, D. A.; MALLIARAS, G. G. Steady-state and transient behavior of organic electrochemical transistors. **Advanced Functional Materials**, Wiley Online Library, v. 17, n. 17, p. 3538–3544, 2007.

45 RIVNAY, J. *et al.* Organic electrochemical transistors with maximum transconductance at zero gate bias. **Advanced Materials**, Wiley Online Library, v. 25, n. 48, p. 7010–7014, 2013.

46 SHIRINSKAYA, A. *et al.* Numerical modeling of an organic electrochemical transistor. **Biosensors**, Multidisciplinary Digital Publishing Institute, v. 8, n. 4, p. 103, 2018.

47 PRIGODIN, V. *et al.* Electric field control of charge transport in doped polymers. **Synthetic Metals**, Elsevier, v. 153, n. 1-3, p. 157–160, 2005.

48 ROBINSON, N. D. *et al.* On the current saturation observed in electrochemical polymer transistors. **Journal of the Electrochemical Society**, IOP Publishing, v. 153, n. 3, p. H39, 2006.

49 PRIGODIN, V. *et al.* Electron-ion interaction in doped conducting polymers. **Physical Review B**, APS, v. 78, n. 3, p. 035203, 2008.

50 TYBRANDT, K.; ZOZOULENKO, I. V.; BERGGREN, M. Chemical potential–electric double layer coupling in conjugated polymer–polyelectrolyte blends. **Science Advances**, American Association for the Advancement of Science, v. 3, n. 12, p. eaao3659, 2017.

51 SZYMAŃSKI, M. Z.; TU, D.; FORCHHEIMER, R. 2-d drift-diffusion simulation of organic electrochemical transistors. **IEEE Transactions on Electron Devices**, IEEE, v. 64, n. 12, p. 5114–5120, 2017.

52 SIDERIS, P.; SISKOS, S.; MALLIARAS, G. Verilog-a modeling of organic electrochemical transistors. *In*: IEEE. INTERNATIONAL CONFERENCE ON MODERN CIRCUITS AND SYSTEMS TECHNOLOGIES (MOCAST), 6., 2017, Thessaloniki. **Proceedings** [...]. Thessaloniki: Aristotle University Research Dissemination Center, 2017. p. 1–4.

53 COPPEDÉ, N.; VILLANI, M.; GENTILE, F. Diffusion driven selectivity in organic electrochemical transistors. **Scientific Reports**, Nature Publishing Group, v. 4, n. 1, p. 1–7, 2014.

54 FRIEDLEIN, J. T. *et al.* Microsecond response in organic electrochemical transistors: exceeding the ionic speed limit. **Advanced Materials**, Wiley Online Library, v. 28, n. 38, p. 8398–8404, 2016.

55 FRIEDLEIN, J. T. *et al.* Optical measurements revealing nonuniform hole mobility in organic electrochemical transistors. **Advanced Electronic Materials**, Wiley Online Library, v. 1, n. 11, p. 1500189, 2015.

56 FARIA, G. C.; DUONG, D. T.; SALLEO, A. On the transient response of organic electrochemical transistors. **Organic Electronics**, Elsevier, v. 45, p. 215–221, 2017.

57 GENTILE, F. *et al.* A theoretical model for the time varying current in organic electrochemical transistors in a dynamic regime. **Organic Electronics**, Elsevier, v. 35, p. 59–64, 2016.

58 GENUCHTEN, M. T. V. **Analytical solutions of the one-dimensional convective-dispersive solute transport equation**. Minnesota: US Department of Agriculture, Agricultural Research Service, 1982.

59 BROWN, R. A brief account of microscopical observations made in the months of june, july and august 1827, on the particles contained in the pollen of plants; and on the general existence of active molecules in organic and inorganic bodies. **The Philosophical Magazine**, Taylor & Francis, v. 4, n. 21, p. 161–173, 1828.

60 SEARS, F. W.; SALINGER, G. L.; LEE, J. E. **Thermodynamics, kinetic theory, and statistical thermodynamics**. Illinois: Addison-Wesley, 1975.

61 SELBERHERR, S. **Analysis and simulation of semiconductor devices**. Vienna: Springer Science & Business Media, 1984.

62 FICK, A. On liquid diffusion. **Journal of Membrane Science**, Elsevier, v. 100, n. 1, p. 33–38, 1995.

63 KRAUME, M. **Transportvorgänge in der Verfahrenstechnik**. Berlin: Springer, 2004.

64 BERGETHON, P. R. **The physical basis of biochemistry:** the foundations of molecular biophysics. Vienna: Springer Science & Business Media, 2013.

65 STEIN, W. **Transport and diffusion across cell membranes**. Amsterdam: Elsevier, 2012.

66 SUNDÉN, B. **Hydrogen, batteries and fuel cells**. Cambridge: Academic Press, 2019.

67 NERNST, W. Zur kinetik der in lösung befindlichen körper. **Zeitschrift für Physikalische Chemie**, De Gruyter Oldenbourg, v. 2, n. 1, p. 613–637, 1888.

68 PLANCK, M. Ueber die erregung von electricität und wärme in electrolyten. **Annalen der Physik**, Wiley Online Library, v. 275, n. 2, p. 161–186, 1890.

69 EINSTEIN, A. Über die von der molekularkinetischen theorie der wärme geforderte bewegung von in ruhenden flüssigkeiten suspendierten teilchen. **Annalen der Physik**, v. 4, 1905.

70 MARIANI, F. *et al.* Microscopic determination of carrier density and mobility in working organic electrochemical transistors. **Small**, Wiley Online Library, v. 15, n. 42, p. 1902534, 2019.

71 COLUCCI, R. *et al.* Recent advances in modeling organic electrochemical transistors. **Flexible and Printed Electronics**, IOP Publishing, v. 5, n. 1, p. 013001, 2020.

72 NEWMAN, J.; THOMAS-ALYEA, K. E. **Electrochemical systems**. New Jersey: John Wiley & Sons, 2012.

73 ELIAZ, N.; BANKS-SILLS, L. Chemical potential, diffusion and stress–common confusions in nomenclature and units. **Corrosion Reviews**, Walter de Gruyter GmbH & Co. KG, v. 26, n. 2-3, p. 87–103, 2008.

74 BHADESHIA, H. A commentary on: Diffusion of carbon in austenite with a discontinuity in composition. **Metallurgical and Materials Transactions A**, Springer, v. 41, n. 7, p. 1605–1615, 2010.

75 DARKEN, L. S. Diffusion of carbon in austenite with a discontinuity in composition. **Transactions of the Metallurgical Society of AIME**, v. 180, p. 430–438, 1949.

76 SUN, B. *et al.* Enhanced mobility of poly (3-hexylthiophene) transistors by spin-coating from high-boiling-point solvents-dtu orbit. **Chemistry of Materials**, v. 16, n. 23, p. 4772–4776, 2004.

77 CHU, P.-H. *et al.* Enhanced mobility and effective control of threshold voltage in p3ht-based field-effect transistors via inclusion of oligothiophenes. **ACS Applied Materials & Interfaces**, ACS Publications, v. 7, n. 12, p. 6652–6660, 2015.

78 GENTILE, F. *et al.* A theoretical model for the time varying current in organic electrochemical transistors in a dynamic regime. **Organic Electronics**, Elsevier, v. 35, p. 59–64, 2016.

79 SHIRINSKAYA, A. *et al.* Numerical modeling of an organic electrochemical transistor. **Biosensors**, Multidisciplinary Digital Publishing Institute, v. 8, n. 4, p. 103, 2018.

80 HANZAEE, F. F. *et al.* A DC model for organic electrochemical transistors and analysis of their performance as voltage amplifiers. *In*: IEEE. INTERNATIONAL MIDWEST SYMPOSIUM ON CIRCUITS AND SYSTEMS (MWSCAS), 64., 2021, Michigan, **Proceedings** [...]. Michigan, 2021. p. 275–278.

81 KAPHLE, V. *et al.* Finding the equilibrium of organic electrochemical transistors. **Nature Communications**, Nature Publishing Group, v. 11, n. 1, p. 1–11, 2020.

82 MACHADO, K. **Eletromagnetismo**. Ponta Grossa: TODAPALAVRA, 2016. v. 2. ISBN 9788562450303.

83 PROCTOR, C. M.; RIVNAY, J.; MALLIARAS, G. G. **Understanding volumetric capacitance in conducting polymers**. New Jersey: Wiley Online Library, 2016. 1433–1436 p.

84 VENKATRAMAN, V. *et al.* Subthreshold operation of organic electrochemical transistors for biosignal amplification. **Advanced Science**, Wiley Online Library, v. 5, n. 8, p. 1800453, 2018.

85 COLUCCI, R. *et al.* Recent advances in modeling organic electrochemical transistors. **Flexible and Printed Electronics**, IOP Publishing, v. 5, n. 1, p. 013001, 2020.

86 SCHIFF, J. L. **The Laplace transform:** theory and applications. Berlin: Springer Science & Business Media, 1999.

87 STAVROULAKIS, I. P.; TERSIAN, S. A. **Partial differential equations:** An introduction with Mathematica and MAPLE. Singapore: World Scientific Publishing Company, 2004.

88 HILLEN, T.; LEONARD, I. E.; ROESSEL, H. V. **Partial differential equations:** theory and completely solved problems. North Dakota: FriesenPress, 2019.

89 MAZUMDER, S. **Numerical methods for partial differential equations:** finite difference and finite volume methods. Cambridge: Academic Press, 2015.

90 FERZIGER, J. H.; PERIĆ, M.; STREET, R. L. **Computational methods for fluid dynamics**. Berlin: Springer, 2002. v. 3.

91 HOFFMANN, K. A.; CHIANG, S. T. **Computational fluid dynamics**. Austin: Engineering Education System, 2000. v. 1.

92 TU, D.; FABIANO, S. Mixed ion-electron transport in organic electrochemical transistors. **Applied Physics Letters**, AIP Publishing LLC, v. 117, n. 8, p. 080501, 2020.

93 SAKURAI, J. J. **Modern quantum mechanics**. Reading, MA: Addison-Wesley, 1994.

94 SQUIRES, G. L.; SQUIRES, G. L. **Practical physics**. Cambridge: Cambridge university press, 2001.

95 CHANG, C.-C. *et al.* Cross-linked triarylamine-based hole-transporting layer for solution-processed PEDOT:PSS-free inverted perovskite solar cells. **ACS Applied Materials & Interfaces**, ACS Publications, v. 10, n. 25, p. 21466–21471, 2018.

96 CAI, H.-T. *et al.* Intrinsic ambipolar transport for the traditional conducting or hole transport ionic blend polymer PEDOT:PSS. **Polymer**, Elsevier, v. 180, p. 121732, 2019.

97 MARKIN, V. S.; VOLKOV, A. G. The gibbs free energy of ion transfer between two immiscible liquids. **Electrochimica Acta**, Elsevier, v. 34, n. 2, p. 93–107, 1989.

98 JIMISON, L. H. *et al.* Measurement of barrier tissue integrity with an organic electrochemical transistor. **Advanced Materials**, Wiley Online Library, v. 24, n. 44, p. 5919–5923, 2012.

99 SERGEEVA, A. S.; GORIN, D. A.; VOLODKIN, D. V. In-situ assembly of ca–alginate gels with controlled pore loading/release capability. **Langmuir**, ACS Publications, v. 31, n. 39, p. 10813–10821, 2015.

Appendices

A Analytic solution of the Nernst-Planck equation

The analytic solution for Eq. (2.28) is well-defined in the literature for different situations.[58] Here, the solution that represents the scenario simulated in Coppede's model will be presented. Therefore, the partial differential equation to be solved is expressed as follows (see Eq. (2.28)):

$$R\frac{\partial\psi}{\partial t} = D\frac{\partial^2\psi}{\partial x^2} - \gamma\frac{\partial\psi}{\partial x}\,. \tag{A.1}$$

In order to obtain a solution for Eq. (A.1), the following boundary and initial conditions are considered:

$$\psi(x,0) = \begin{cases} \psi_1 & 0 < x < x_1 \\ \psi_2 & x > x_1 \end{cases} \tag{A.2}$$

$$\psi(0,t) = \begin{cases} \psi_0 & 0 < t < t_0 \\ 0 & t > t_0 \end{cases} \tag{A.3}$$

$$\frac{\partial\psi}{\partial x}(\infty,t) = 0\,. \tag{A.4}$$

In this case, the solution can be defined as:

$$\psi(x,t) = \begin{cases} \psi_2 + (\psi_1 - \psi_2)A(x,t) + (\psi_0 - \psi_1) & 0 < t < t_0 \\ \psi_2 + (\psi_1 - \psi_2)A(x,t) + (\psi_0 - \psi_1) - \psi_0 B(t - t_0) & t > t_0\,, \end{cases} \tag{A.5}$$

where

$$\begin{aligned} A(x,t) =& \frac{1}{2}\mathrm{erfc}\left[\frac{R(x-l)-\gamma t}{2\sqrt{DRt}}\right] + \frac{1}{2}e^{\gamma x/D}\mathrm{erfc}\left[\frac{R(x+l)+\gamma t}{2\sqrt{DRt}}\right] \\ B(x,t) =& \frac{1}{2}\mathrm{erfc}\left[\frac{Rx-\gamma t}{2\sqrt{DRt}}\right] + \frac{1}{2}e^{\gamma x/D}\mathrm{erfc}\left[\frac{Rx+\gamma t}{2\sqrt{DRt}}\right] \end{aligned} \tag{A.6}$$

$$\begin{aligned} \mathrm{erf}(t) &= \frac{2}{\sqrt{\pi}}\int_0^t e^{-\tau^2}\mathrm{d}\tau \\ \mathrm{erfc}(t) &= 1 - \mathrm{erf}(t)\,. \end{aligned} \tag{A.7}$$

Solutions for a different set of boundary and initial conditions can be found in the work of

Van Genuchten, *et. al.*[58]

B Stability Analysis for Fick's Second Law

In this section, an analysis of the stability condition for the diffusion equation (see Section 2.1) is developed. If an evenly spaced grid is considered, i.e. $\Delta x_{k+1} = \Delta x_k$, Eq. (2.46) turns into:

$$\left(\frac{\partial^2 f(x)}{\partial x^2}\right)_{x=x_k} \approx \frac{f(x_k + \Delta x_{k+1}) - 2f(x_k) + f(x_k - \Delta x_{k+1})}{\Delta x^2} \,. \tag{B.1}$$

Using Eq. (B.1) and forward differences in time, the algebraic manipulation of second Fick's law (see Section 2.1) leads to:

$$\psi_k^{l+1} = \psi_k^l + D\frac{\Delta t}{\Delta x^2}(\psi_{k+1}^l - 2\psi_k^l + \psi_{k-1}^l) \,. \tag{B.2}$$

Here, the notation $\psi_k^l = \psi(x_k, t_l)$ and $\psi_{k\pm1}^l = \psi(x_k \pm \Delta x, t_l)$ is introduced. In order to solve Eq. (B.2), the following solution is assumed:

$$\psi_k^l = (\zeta)^l e^{i\epsilon(k\Delta x)} \,, \tag{B.3}$$

where $i = \sqrt{-1}$ and ϵ is referred as the wavenumber of the solution mode, which can take any value. In this solution, ζ raised to lth power is the unknown parameter that has to be determined. If for any k, $|\zeta| > 1$, it is said that the scheme is unstable, which means that the previous expression will tend to infinity as the time index l is increases. The substitution of Eq. (B.3) into Eq. (B.2) gives:

$$(\zeta)^{l+1} e^{i\epsilon(k\Delta x)} = (\zeta)^l e^{i\epsilon(k\Delta x)} + D\frac{\Delta t}{\Delta x^2}((\zeta)^l e^{i\epsilon(k+1)\Delta x} - 2(\zeta)^l e^{i\epsilon(k\Delta x)} + (\zeta)^l e^{i\epsilon(k-1)\Delta x}) \,. \tag{B.4}$$

Dividing by $(\zeta)^l e^{i\epsilon(k\Delta x)}$, the result may be expressed as follows:

$$\zeta = 1 + D\frac{\Delta t}{\Delta x^2}(e^{ik\Delta x} - 2 + e^{-ik\Delta x}). \tag{B.5}$$

Using the definition $e^{ik\Delta x} + e^{-ik\Delta x} = 2\cos(kx\Delta)$, the latest result turns into:

$$\zeta = 1 + D\frac{2\Delta t}{\Delta x^2}(\cos(kx\Delta) - 1) \,. \tag{B.6}$$

Here, it is observed that the maximum negative value that the second term on the right side of Eq. (B.6) can achieve, is in the case that $\cos(kx\Delta) = -1$. Therefore, in order to investigate

in which cases the scheme is unstable, the conditions where $\zeta < -1$ are analyzed. Thus, the condition:

$$1 - \frac{4\Delta t D}{\Delta x^2} < -1 \, . \tag{B.7}$$

leads to

$$\Delta t < \frac{\Delta x^2}{2D} \, , \tag{B.8}$$

which is the stability criterion for Fick's second law when the explicit method considering a uniform grid is implemented. From Eq. (B.8) it is observed that in this case, the parameter Δt depends on the values Δx and D.

C Solution of Fick's second law

For pure diffusion processes, the governing equation is defined by the second Fick's law, which may be expressed as (see Section 2.1):

$$\frac{\partial \psi(x,t)}{\partial t} = D \frac{\partial^2 \psi(x,t)}{\partial x^2} \, . \tag{C.1}$$

Aiming to solve the previous equation, the boundary condition $\psi(x \to \pm\infty, t) = 0$ for $t > 0$ is implemented. As it is of interest to study the case presented in the Section 3.4, a concentration contribution located at one single point x_0 is considered. Thus, in this situation results useful to define the initial condition as a delta distribution, i.e. $\psi(x,0) = \delta(x - x_0)$. A well-known tool used to solve partial differential equations is the Fourier transform. Hence, given a function $\psi(x,t)$, the Fourier transform in relation to space gives a function $\hat{\psi}(\omega,t)$ in the space of frequency ω as follows:

$$\mathscr{F}(\psi(x,t)) = \hat{\psi}(\omega,t) = \frac{1}{\sqrt{2\pi}} \int_{-\infty}^{\infty} \psi(x,t) e^{-ix\omega} dx \, . \tag{C.2}$$

For the spatial derivatives, the transform can be expressed as:

$$\mathscr{F}\left(\frac{\partial \psi(x,t)}{\partial x}\right) = i\omega \hat{\psi}(\omega,t) \tag{C.3}$$

$$\mathscr{F}\left(\frac{\partial^2 \psi(x,t)}{\partial x^2}\right) = -\omega^2 \hat{\psi}(\omega,t) \, . \tag{C.4}$$

In addition, the calculation of the transform for the temporal derivative leads to:

$$\mathscr{F}\left(\frac{\partial\psi(x,t)}{\partial t}\right)=\frac{1}{\sqrt{2\pi}}\int_{-\infty}^{\infty}\frac{\partial\psi(x,t)}{\partial t}e^{-ix\omega}dx=\frac{1}{\sqrt{2\pi}}\frac{\partial}{\partial t}\int_{-\infty}^{\infty}\psi(x,t)e^{-ix\omega}dx=\frac{\partial}{\partial t}\hat{\psi}(\omega,t)\,. \tag{C.5}$$

Applying Fourier transform for the spatial coordinate to Eq. (2.2), it can be expressed as:

$$\frac{\partial}{\partial t}\hat{\psi}(\omega,t)+D\omega^2\hat{\psi}(\omega,t)=0\,, \tag{C.6}$$

which now is an ordinary differential equation in time for each value of ω. Multiplying both sides by the integration factor $e^{D\omega^2 t}$, Equation (C.6) turns into:

$$\frac{\partial}{\partial t}\left(e^{D\omega^2 t}\hat{\psi}(\omega,t)\right)=0\,. \tag{C.7}$$

If the latest result is integrated with respect to t but maintaining a fixed ω, it is obtained the following result:

$$\hat{\psi}(\omega,0)-e^{D\omega^2 t}\hat{\psi}(\omega,t)=0\Rightarrow\hat{\psi}(\omega,t)=\hat{\psi}(\omega,0)e^{-D\omega^2 t}\,, \tag{C.8}$$

where, $\hat{\psi}(\omega,0)$ represents the transform of the initial condition $\psi(x,0)$ imposed on the system. Using the definition of the Fourier transform for a delta function $\mathscr{F}(\delta(x-x_0))=\frac{1}{\sqrt{2\pi}}e^{-\omega i x_0}$, the result may be expressed as follows:

$$\hat{\psi}(\omega,t)=\frac{1}{\sqrt{2\pi}}e^{-D\omega^2 t}e^{-\omega i x_0}\,, \tag{C.9}$$

Now, applying the inverse Fourier transform, the solution can be defined in the space domain again. Thus, the following result is obtained:

$$\psi(x,t)=\mathscr{F}^{-1}(\hat{\psi}(\omega,t))\,. \tag{C.10}$$

From the definition of the inverse transform, $\psi(x,t)$ is found to be:

$$\psi(x,t)=\frac{1}{\sqrt{2\pi}}\int_{-\infty}^{\infty}\hat{\psi}(\omega,t)e^{ix\omega}d\omega=\frac{1}{2\pi}\int_{-\infty}^{\infty}e^{-D\omega^2 t}e^{-\omega i x_0}e^{ix\omega}d\omega=\frac{1}{2\pi}\int_{-\infty}^{\infty}e^{-D\omega^2 t+i(x-x_0)\omega}\cdot d\omega \tag{C.11}$$

By doing algebraic manipulations of the exponent $-D\omega^2 t+i(x-x_0)\omega$, one may express it as

$$\begin{aligned}-Dt(\omega^2-\frac{i(x-x_0)}{Dt}\omega)&=-Dt\left(\omega^2-\frac{i(x-x_0)}{Dt}\omega+\frac{i^2(x-x_0)^2}{(2Dt)^2}-\frac{i^2(x-x_0)^2}{(2Dt)^2}\right)\\&=-\frac{(x-x_0)^2}{4Dt}-Dt\left(\omega-\frac{i(x-x_0)}{2Dt}\right)^2\,,\end{aligned} \tag{C.12}$$

which allows to develop a change in the variables of the integration. Therefore:

$$y = \sqrt{Dt}\left(\omega - \frac{i(x-x_0)}{2Dt}\right) \Rightarrow dy = \sqrt{Dt}d\omega \,. \tag{C.13}$$

Inserting the previous result in Equation (C.11) leads to:

$$\psi(x,t) = \frac{1}{2\pi} e^{-\frac{(x-x_0)^2}{4Dt}} \int_{-\infty}^{\infty} e^{-y^2} \frac{dy}{\sqrt{Dt}} \,. \tag{C.14}$$

As $\int_{-\infty}^{\infty} e^{-y^2} dy = \sqrt{\pi}$, the solution of Fick's second law is:

$$\psi(x,t) = \frac{1}{\sqrt{4\pi Dt}} e^{-\frac{(x-x_0)^2}{4Dt}} \,, \tag{C.15}$$

which is indeed the Eq. (3.8) in the main text.

D Steady-state solution for Drift-Diffusion

In the case at which a system has achieved the steady state, the concentration profile is no longer changing, which means that $\frac{\partial \psi}{\partial t} = 0$. Therefore, in order to obtain the steady state solution for the Nernst-Planck equation (see Eq. (2.1)), the condition $\frac{\partial \psi}{\partial t} = 0$ is implemented. Thus, Equation (2.7) for a uniform electric field E is expressed as:

$$0 = -D\left(\frac{\partial^2 \psi}{\partial x^2} - \frac{zeE}{k_B T^a}\frac{\partial \psi}{\partial x}\right) . \tag{D.1}$$

Now, it is considered a solution for Equation (D.1) that has the form:

$$\psi = Ae^{bx} \,, \tag{D.2}$$

where, A is a normalization factor and b is a constant to be determined. Inserting Eq. (D.2) in Eq. (D.1), leads to:

$$0 = -b^2\psi + \frac{zeE}{k_B T^a} b\psi \,. \tag{D.3}$$

Solving for b, it is obtained the following result:

$$b = \frac{zeE}{k_B T} \,. \tag{D.4}$$

Then, the function assumed for ψ solves the differential equation. Note that the solution depends explicitly on the electric field applied. In order to determine the normalization factor A, the conservation of the total number of particles is considered. Initially, the system has a concentration $\psi_0 = \psi(x,0)$, which have to be conserved at all times. Therefore, the conservation of particles for a system with length L establish that:

$$\int_0^L \psi dx = \int_0^L \psi_0 dx = N_0 = \text{cte} \, . \tag{D.5}$$

The calculation of the integral on the left side of the previous relation leads to:

$$\frac{A}{\omega} \left[e^{bL} - 1 \right] = N_0 \, . \tag{D.6}$$

Solving the latest result for A allow to obtain:

$$A = \frac{b}{\left[e^{bL} - 1 \right]} N_0 \, . \tag{D.7}$$

Therefore, the analytical solution for Nernst-Planck equation in the steady-state is established as a function that presents an exponential profile.